DYNAMIC COMPLIANT WALKING OF THE SCOUT II QUADRUPED

Martin de Lasa

Department of Electrical and Computer Engineering
McGill University, Montréal, Canada

A Thesis submitted to the Faculty of Graduate Studies and Research in partial fulfillment of the requirements of the degree of
Master of Engineering

Abstract

This research presents the development of a novel dynamic walking controller for a simple quadrupedal robot, *Scout II*. Since Scout II does not have knees, a modified version of the bound, which we call a walking bound was studied. To gain understanding of system behaviour, an iterative approach of simulation, analysis, and experimentation was pursued. First a simulation study used in the development of rocking and walking controllers was undertaken. Attempts to experimentally implement the mentioned controllers revealed unmodelled dynamics having significant effects on system behaviour. Therefore, another walking algorithm based on commanding constant hip velocity was experimentally developed. This algorithm proved successful, yielding stable walking for narrow ranges of operating conditions despite a simple open loop strategy using minimal feedback. Typical mechanical and electrical power, as well as specific resistance for Scout II compliant walking are quantified.

Résumé

Cette thèse présente le dévelopement d'un nouveau contrôleur de marche dynamique pour *Scout II*, un robot quadrupède simple. Puisque Scout II n'a pas de genoux, nous avons dévelopé une marche dans laquelle les paires de jambes antérieures et postérieures fonctionnent ensemble. Pour mieux comprendre le comportement de ce système, nous avons utilisé une méthode itérative de simulation, d'analyse et d'expérimentation. D'abord nous avons simulé deux algorithmes de marche qui nous ont aidés à mieux comprendre le comportement du système. Néanmoins, à cause de facteurs dynamiques inattendus, ces algorithmes n'ont pas fonctionnés sur notre plateforme expérimentale. Nous avons donc dévelopé un autre contrôleur, cette fois experimentalement, dont le but était de commander une vitesse constante aux hanches du robot. Cet algorithme a bien fonctionné pour une série de conditions limitées, même si c'était un contrôleur simple à boucle ouverte. La puissance mécanique et électrique, et la résistance spécifique de Scout II ont aussi été mesurées.

Acknowledgements

Throughout the course of my research I have received immeasurable guidance, support, and friendship from numerous individuals. In particular I would like to thank :

- Professor Martin Buehler, my supervisor, for his help and guidance through the course of my thesis. Martin's approach to research and willingness to tackle the daily obstacles I encountered, were sources of support and encouragement for me. His efforts to make the ARL a fun and motivating place to work made my graduate experience a memorable one.

- The Natural Sciences and Engineering Research Council of Canada (NSERC) for their support of my work through a graduate scholarship.

- Shervin Talebi, a good friend and irreplaceable colleague. Shervin was always up for a good debate and willing to have me bounce ideas off him. His help and generosity in all aspect of my research can not be overstated.

- Geoff Hawker for maintaining the lab's PC in running order, getting QNX running on Scout, and for helping to make the four o'clock Quake deathmatch an ARL ritual.

- Dave McMordie for reenergizing the ARL and showing all of us that there is no shame in frying electronics. Dave's positive attitude, unending imagination, and energy are an inspiration to me.

- Robert Battaglia for building an excellent robotic platform that we have all benefited from. Scout has managed to take considerable abuse and

grief from various "trainers" and still manages to amazes us with its gracefulness and animal like qualities.

- Ken Yamazaki, for welcoming me into the ARL family and letting me shadow him when I was still wet behind the ears. Ken's quiet disposition and kindness made me feel at home from the time I arrived in the lab.

- Mojtaba Ahmadi for his kindness to me when I first joined the ARL. Mojtaba did not hesitate to help make my move to Montreal a pleasant one.

- Don Campbell for his excellent work on Scout's electronics. Starting with the now irreplacable IR module and onto more recent projects, I have had a great time working with him.

- Sami Obaid for his work on Scout's sensors and electronics. His work was an invaluable resource in the electronics design stage of my thesis. Sami always lit up the lab with his energy and warmth.

- Didier Papadopoulos for his breakthrough work with Scout. Didier helped give all of us hope that one day our locomotion algorithms would also work.

- Ned Moore for making sure we always had some music to lighten up the lab.

- Liana Mitrea for all her kind gestures and for always bringing something sweet to the lab for us to enjoy.

- CIM's current and past secretarial staff : Ornella Cavaliere, Cynthia Davidson, and Kathleen Vandernoot for helping with rush courier deliveries, emergency faxes and kind smiles.

- Marlene Gray, CIM's manager, for her support and friendship. Marlene always made sure to drop in and check that things were advancing. Her small attentions did not go unnoticed.

- Jan Binder, CIM's network administrator, for keeping the computer network running smoothly and saving me from a few unexpected deletes of the lab web page.

- To my family and new parents in law who supported me through this often difficult experience, thank you for your love and support.

- Lastly I would like to especially thank my wife Magdalena Krol. Her support, encouragement, and confidence in me through the more testing times of my Master's, helped make this thesis a reality. Her contributions are beyond words.

Contents

List of Figures

List of Tables

Chapter 1

Introduction

1.1 Overview

According to Raibert, only half of the earth's land mass is currently accessible by wheeled or tracked vehicles, with a much larger fraction being accessible to legged creatures. Even the indoor environments that humans routinely navigate through effortlessly can present major challenges to wheeled and tracked robotic platforms. From this perspective, the development and study of legged robots offers many potential advantages. Whereas wheeled or tracked vehicles are restricted by the worst terrain they must traverse, requiring a continuous path of support for their wheels, legged creatures are limited by the best footholds in the reachable terrain [54]. In addition, legs can serve as an active suspension system helping to decouple terrain variations from body movements thus smoothing locomotion.

Compelling scientific arguments exist for the development and study of legged robotic systems. Doing so may provide insight helping to better understand the locomotion strategies adopted by animals. Hypotheses developed from the study of legged robots can be tested against studies of animal locomotion. Conversely, studies and observations of animals can provide guidance, helping to yield better robot designs.

Design and control of these systems also presents some unique challenges, making them interesting engineering case studies. As with any complex project, design and integration issues must be addressed requiring an understanding of the roles played by the various system components (i.e. electrical, mechanical, software). Other design and implementation requirements such as sensing, actuation, and power distribution for mobile robots are more domain specific, given the additional need of legged robots for untethered autonomous operation. In the area of control, the nonlinearity and discontinuous dynamic nature of legged robots make them ideal testbeds and motivators for new control theory.

Regardless of the motivation for studying legged robots one thing is clear : If modern robotics is ever to fulfill its promise, a means will need to be provided for robots to operate in the world humans have created for themselves. Legs are the natural choice.

1.2 Motivation

Motivated by a desire to mimic the agility of animals, legged robotics research has traditionally focused on the study and implementation of systems with many actuated degrees of freedom. Unfortunately, this has often yielded robotic systems whose full range of motion was difficult to exploit, due to high system complexity, high weight, and to a lack of formal methods for the development of robust control schemes.

To investigate the potential of low actuated degree of freedom legged platforms, the development of walking algorithms for an underactuated compliant legged quadrupedal robot *Scout II* was studied.

Studying simple legged robotic platforms has several advantages :

- Dominant dynamic factors influencing mammalian and robot locomotion can be identified.

- The study of locomotion energetics helps guide future robots designs by pin-pointing actuators that are crucial or redundant.
- Systems can be designed and studied with complexity added incrementally.
- A practical body of control techniques and theory can be developed. This work can later be used as the basis of control for more complicated robots.

The reduction in system complexity resulting from a straightforward robot design also achieves another, perhaps more important, goal :

- Cost is lowered and reliability is increased while achieving mobility sufficient for many robotic task domains.

We believe that these characteristics will help bring legged robots out of the research lab and into the real world.

1.3 Approach

Although studying simple legged robots offers many potential advantages, it imposes significant restrictions on researchers and designers of locomotion algorithms by limiting control inputs. Further constraints are placed on control design, since the need for autonomous untethered operation also dictates that actuator weight must be kept low to help prolong operation life of these systems.

These design constraints force control engineers to use actuators in peak power regions, where available torque is usually a function of velocity. Even if the desired torque is available, slip between the toe and the ground limits the torque that can be applied.

These control complexities and input limitations justify the approach taken in this thesis: *controller development informed by simulations, intuition and extensive experimentation.*

1.4 Contributions

This thesis contains the following original contributions :

- The role of front and back legs in Scout II quadrupedal walking were identified.
- A novel open-loop compliant walking controller was developed and validated experimentally on Scout II.
- Input electrical and output mechanical power were measured and formally discussed for the first time on Scout II.
- Specific resistance was determined for walking in a narrow range of velocities.

1.5 Thesis Organisation

This thesis is divided in the following manner :

Chapter 2 presents a literature review of key research done to date on legged robots. Although no work exists on the development of dynamic walking algorithms for quadrupedal robots with only one actuator per leg, literature in the closely related areas of control of running robots, control of walking robots with articulated legs, and control of passive dynamic robots is surveyed. A review of animal gaits is also presented to familiarise the reader with relevant terminology.

Chapter 3 discusses system level decisions made during design and implementation of Scout II's electronic and software subsystem, undertaken as part of this thesis.

Chapter 4 presents a planar model used to perform numerical simulations of underactuated quadrupedal walking. To simplify the task of controller development and to gain insight into system behaviour, rocking was first studied. The designed rocking controller was then modified, yielding stable walking. Modeling considerations are discussed.

Chapter 5 reports experimental results from tests of the developed control strategies on Scout II. Preliminary experiments revealed errors in modeling assumptions, which did not allow the rocking and walking controllers of chapter 4 to be used. Instead another controller was experimentally developed, yielding stable walking. Analysis revealed lossy dynamics and implementation limitations, helping to explain the failure of the rocking algorithm. To quantify system energetics, mean electrical and mechanical power was measured. These values were then used to calculate the corresponding specific resistance for walking in a narrow velocity range.

Chapter 6 summarises important findings of this thesis, enumerating possible directions for future research.

Chapter 2

Background

2.1 Overview

This chapter presents background information relevant to the understanding of locomotion and control of legged robots. Section 2.2 presents an overview of animal locomotion to familiarise the reader with terminology used in the fields of biology and robotics. Sections 2.3 and 2.4 present related research used as a starting point for the work presented in this thesis.

2.2 Animal Locomotion Gaits

The scientific study of legged locomotion began in the later half of the 19th century when Leland Stanford, governor of California, breeder of trotting horses, and founder of Stanford University, hired Eadward Muybridge to find out whether or not horses experienced a ballistic phase of motion during trotting. Although Standford eventually lost the wager which had prompted him to hire Muybridge (he claimed horses did not experience flight during trotting), Muybridge's continued his work on gait analysis and later published the first stop frame photographic study of locomotion [54].

Muybridge's analysis demonstrated that quadrupedal animals use several common sequences of foot placements, or gaits, during locomotion. These gaits include : the walk, the amble, the trot, the rack, the canter, and the gallop [45]. The order of gaits correspond to what might be seen in nature when observing a quadruped move from slow to rapid locomotion. Although animals will generally use several of the mentioned gaits, there is probably not a single animal that uses all of them. In their seminal work on gait energetics Hoyt and Taylor [33] showed that animals select their locomotion gait not only to attain a desired speed, but also to minimize oxygen consumption.

A brief description of the above mentioned gaits is provided below. In addition, other less common gaits : the ricochet, the pronk, and the bound are also discussed. These gaits have the distinguishing property of having symmetric patterns of foot placements.

2.2.1 The Walk

The walk is the principal gait of most quadrupedal animals moving at low speeds. Figure 2.1 shows the pattern of successive foot placements during a walk. As can be seen, the walk alternates between having two and three support feet. This causes a pattern of foot placements whereby support during a stride occurs twice on the lateral legs, twice on the diagonals, twice on two fore-feet and one hind foot and twice on two back feet and one fore foot. Walking can also slow to a crawl, a gait that alternates between providing support on three and four feet.

2.2.2 The Amble

The amble is an accelerated walk having the same sequence of foot placements as the walk (refer to figure 2.1). However, given the more rapid movement, support of the body alternates between two feet of support and one. Interestingly, the amble is one of only two gaits along with the walk, used by the

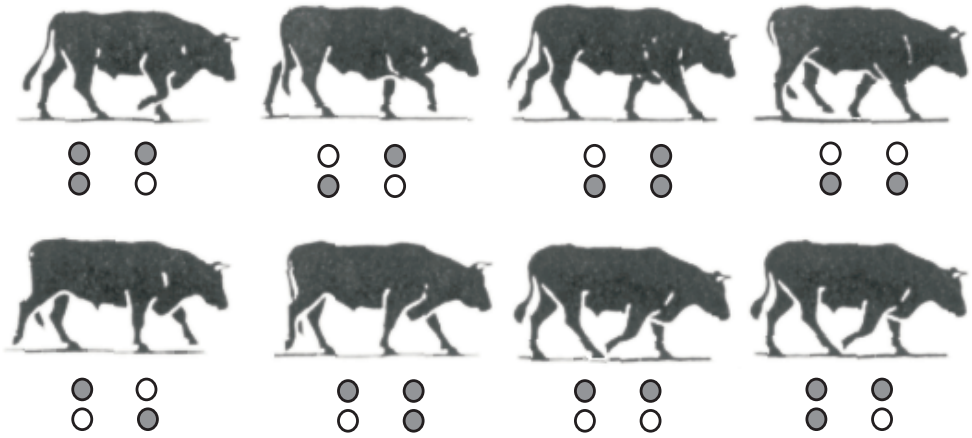

Figure 2.1: Ox in walk gait (adapted from [23]).

elephant in nature.

2.2.3 The Trot

The trot is a gait in which diagonally opposite pairs of feet are alternatively lifted, swung forward, and again placed on the ground. Twice during each stride, the body is ballistic and without support. In the case of some larger animals, this ballistic phase amounts simply to the feet being dragged along the ground, nonetheless the feet are not supporting the body during this phase of motion. Figure 2.2 shows an illustration of a horse in a trotting gait.

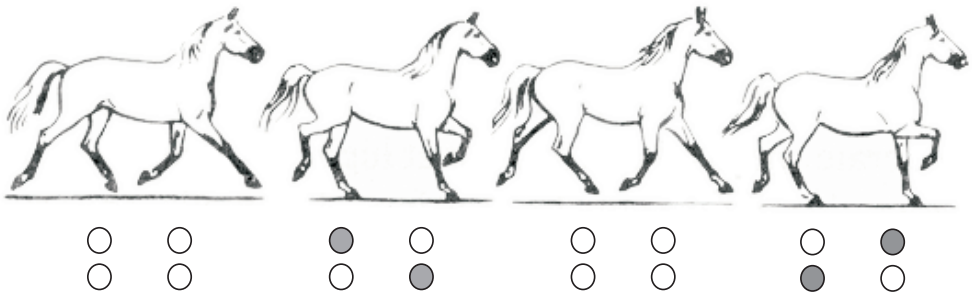

Figure 2.2: Sketch of horse in trot gait. The diagonal pattern of support legs can clearly be seen (adapted from [3]).

2.2.4 The Rack

The rack, or pace, is a gait used by camels, giraffes, and occasionally dogs. During a rack, pairs of legs move in lateral rather than diagonal pairs, such as in the trot. Figure 2.3 shows a simplified diagrammatic representation of the rack. Since this is particularly uncomfortable gait for riders, horses are rarely trained in the use of this gait. The discomfort of the gait is so great that the gait's name is taken from the medieval torture device sharing its name. In profile, the pace is virtually indistinguishable from the trot.

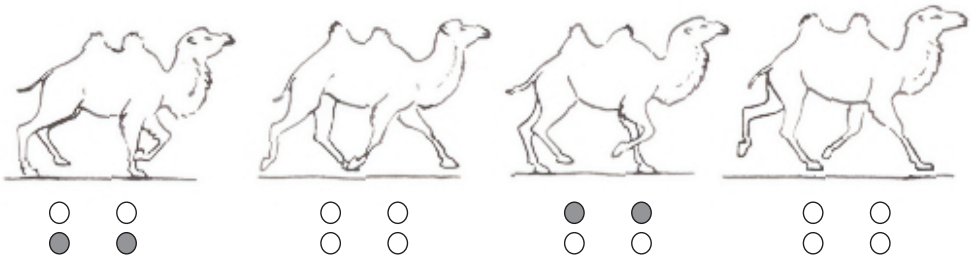

Figure 2.3: Camel in rack gait (adapted from [14]).

2.2.5 The Canter

The canter has the same pattern of foot falls as the walk, but with uneven regularity of intervals and periods of support (see figure 2.4). In a canter the torso of the animal's body begins to experience larger oscillate from the horizontal, causing a slight rocking or canting motion of the body from which the gait's name is taken.

2.2.6 The Gallop

The gallop is the quickest of all quadrupedal animal gaits. There are two different galloping gaits, the transverse-gallop and the rotary-gallop. The transverse-gallop, a gait employed by the horse and by most other hoved and soft-toed animals, is characterised by foot impacts that follow each other in

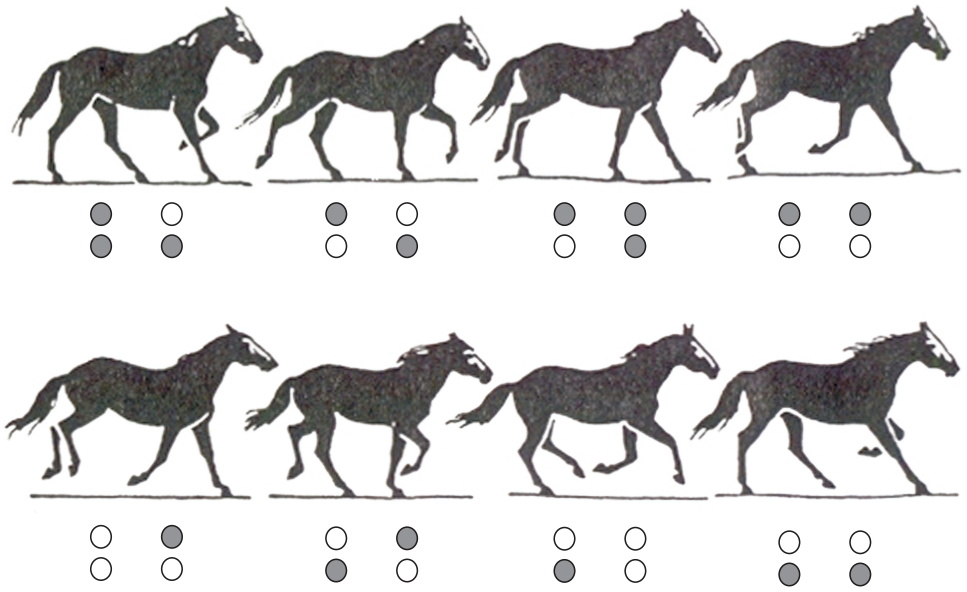

Figure 2.4: Horse in canter gait (adapted from [14]).

what are roughly the points on a cross (see figure 2.5). The rotary-gallop, a gait adopted by dogs, deer, and other animals, has foot falls that follow a circular pattern.

2.2.7 The Ricochet and the Pronk

Some gaits observed in nature have the characteristic of having symmetrical patterns of foot placements during support. Two such gaits which have already been mentioned are the trot and the pace. Some less common gaits used only by a few animals are the ricochet and the pronk.

The ricochet is the gait principally employed by a class of animals such as the kangaroo. The word "ricochet", often used by artillerists to describe the skipping or bouncing of a projectile over land or water, is particularly appropriate in describing this motion. Figure 2.6 shows this gait pattern, excluding the motion of the kangaroo's tail, which in reality contributes significantly in propelling the body forward.

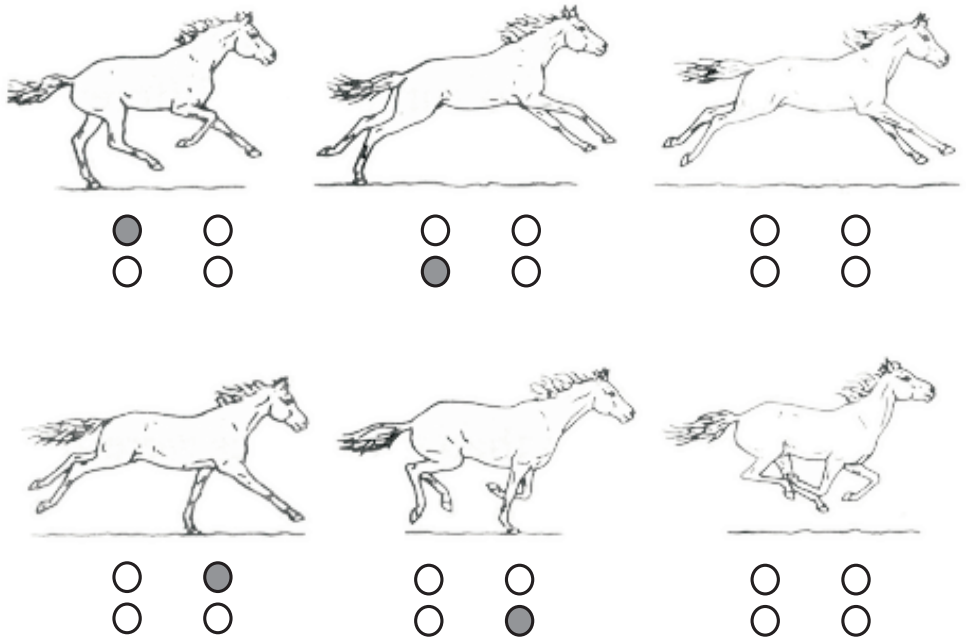

Figure 2.5: Sketch of horse in transverse gallop gait. (adapted from [3]).

The pronk is a gait used by quadrupeds such as deer and gazelle. It is equivalent to the ricochet except that both front and back sets of feet perform the same action. The pronk is the quadrupedal gait providing the largest amount of toe clearance, however it is only passively stable for narrow ranges of body inertias.

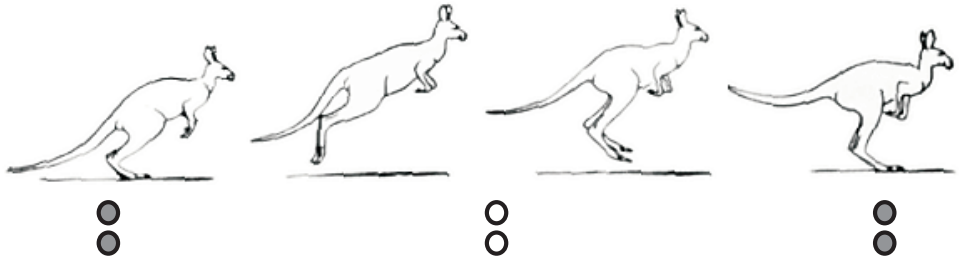

Figure 2.6: Kangaroo in ricochet gait. (adapted from [23]).

2.2.8 The Bound

The bound is a running gait used by a few small quadrupeds such as squirrels, rodents, and dogs. In the bound, support alternates between pairs of legs, with the fore and hind limbs acting in unison to thrust the body forward. Figure 2.7 shows a Siberian souslik in a bound gait. As can be observed from this figure, there is approximately a 180^o phase difference between the sets of front and back legs. This gait is of particular interest since, of all gaits discussed so far, the bound has the shortest gait period, allowing for frequent interactions of the legs with the ground. This makes the bound well suited for obstacle avoidance and for providing propulsion [8]. Simulation analysis first conducted by Murphy [21] and later validated by Neishtadt and Li [47] showed that certain simple planar quadruped bounding models are always passively stable for dimensionless body inertia values of less than one.

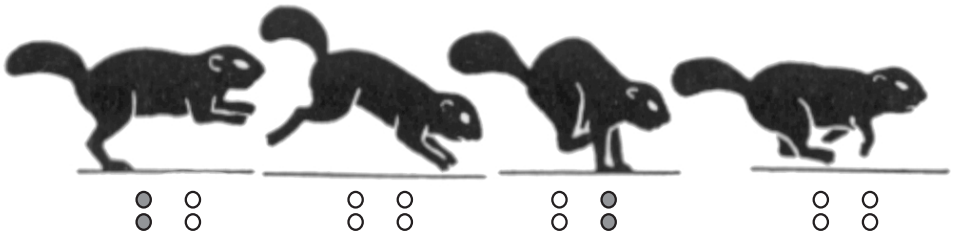

Figure 2.7: Long tailed Siberian souslik in bound gait. (adapted from [14]).

2.3 Control of Legged Robots

Legged robotic systems are divided into two categories : *statically* and *dynamically* stable robots, differing in the mechanism used to maintain stability.

At low speeds, statically stable robots maintain balance by ensuring that the ground projection of the centre of mass (COM) of the robot is contained within the convex polygon formed by the feet in contact with the ground at all times. McGhee and Frank [43] defined the longitudinal stability margin as the shortest distance between the projected COM location and the convex support

polygon boundaries (see figure 2.8). Maintaining the projection of COM inside the support polygon, ensures that the robot will not topple if there are delays in motion or if there is a vehicle power failure. To do this, statically stable robots are typically designed having more than four legs, however statically stable bipeds with large feet have also been built. To minimise the effects of the destabilising forces resulting from the internal energy of reciprocating limbs, statically stable robots usually have legs with a low mass as compared to that of the body.

As the robot's speed begins to increase, the inertia and velocity of a robot's body starts to make the ground projection of the COM a less accurate means of assessing robot stability. To address this problem, energy based stability measures have since been proposed by Messuri and Klein [44] and by Nagy et al. [46].

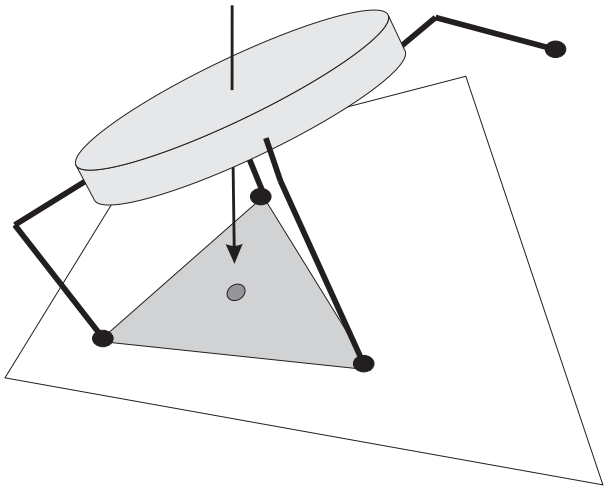

Figure 2.8: A low speeds statically stable robots can maintain stability by keeping the projection of their center of mass, also referred to as the ground projection of the centre of mass (GCM), within the convex hull formed by the support feet.

Statically stable robots designed to date include the Ohio State University Active Suspension Vehicle (OSU-ASV) [42], Ambler [4], Dante II [5], and the SONY Aibo Dog [37] (see figure 2.9).

Statically stable legged robots locomotion speed is typically limited, de-

Figure 2.9: SONY Aibo Dog [17].

pending on geometry, to much less than one body length per second. Dynamically stable robots, on the other hand, are not subject to these constraints and can exploit dynamic forces and feedback to maintain marginal stability in a limit cycle that repeats once each stride.

Unfortunately, dynamically stable robots suffer from a lack of formal control development and analysis techniques, since these systems exhibit discontinuous dynamics at state transitions, are highly nonlinear, are multi-input multi-output, act in gravity fields, and interact with unstructured complex environments. In addition, benchmarks for such systems also differ from more classical measures of performance such as disturbance rejection and command following. Instead, measures such as biological similarity, locomotion smoothness, efficiency, top speed, and robustness are often used [35]. To add to these already significant challenges, controller synthesis can be further complicated since it is often advantageous to limit or reduce actuated degrees of freedom in robot design and instead exploit passive elements, such as springs, to provide compliance.

To date, no work exists on dynamical walking controller design for underactuated quadruped robots with the exceptions of research in three closely related areas: control of dynamic running robots, control of dynamic walking robots with articulated legs, and exploiting passive dynamics in legged robot control. Section 2.4 summarises key work done to date in these areas.

2.4 Control of Dynamically Stable Legged Robots

2.4.1 Control of Running Robots

Given the lack of formal development and control analysis techniques, the largest category of control synthesis approaches used to date in legged robotics has been based on intuition, experimentation, and simulation. Although many dynamic hopping, jumping, and running robots have been developed, a complete review is outside the scope of this thesis. Instead, key control approaches for dynamic legged robots will be addressed.

In the area of running robots Raibert [54] performed arguably some of the most important research to date. Starting with a one legged planar robot, control of running was investigated. A novel strategy was proposed that partitioned control of running into three decoupled parts, synchronised by a leg finite state machine (figure 2.10). Control of hopping height, forward speed and body pitch were treated as three separate control tasks with dynamic coupling treated as system disturbances. Hopping height was regulated by specifying the thrust to be delivered by the leg during stance and forward speed of the robot was controlled by extending the foot to a desired position during flight. Leg touchdown position was calculated by trying to maintain symmetry in running (i.e. placing the foot at half the forward distance travelled by the robot in the previous stride). The third part of the control algorithm applied a hip torque during stance in order to achieve a desired body angle.

Using findings from experiments with the one legged hopper and borrow-

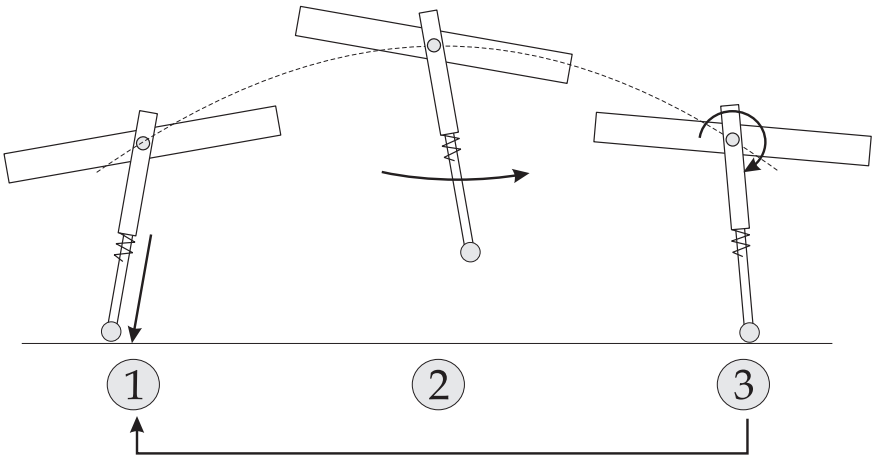

Figure 2.10: Raibert used a simple three part controller in the control of his monopod : 1) A thrust was applied to control vertical hopping height 2) Forward speed was regulated by placing the leg at a desired touchdown position 3) During stance hip torque was applied to achieve a desired body angle.

ing the concept of virtual legs, originally proposed by Sutherland [59], control was later generalised for various other robots including a three dimensional monopod, planar, and three dimensional bipeds, as well as a three dimensional quadruped robot (figure 2.11). Use of virtual legs permitted Raibert to exploit symmetry in certain animal gaits, by grouping legs that acted together into virtual legs and using the tri-partite algorithm on these virtual legs. This strategy allowed the Raibert quadruped to pace, trot, pronk, and bound [1] [55]. A more detailed discussion of the virtual leg concept is presented in chapter 5 in the context of the dynamic walking controller developed for this thesis.

To focus efforts on the task of control and robot design, Raibert eliminated power constraints and used powerful hydraulic actuators, driven by pumps located off the robot. To improve upon the robot energetics Gregorio and Buehler [27, 28], designed an electrically actuated version of the Raibert one-legged hopper called Monopod I (figure 2.12) that significantly reduced power consumption. Ahmadi further refined Monopod I's design, when it was

[1] a description of the pace, trot, pronk and bound gaits can be found in section 2.2

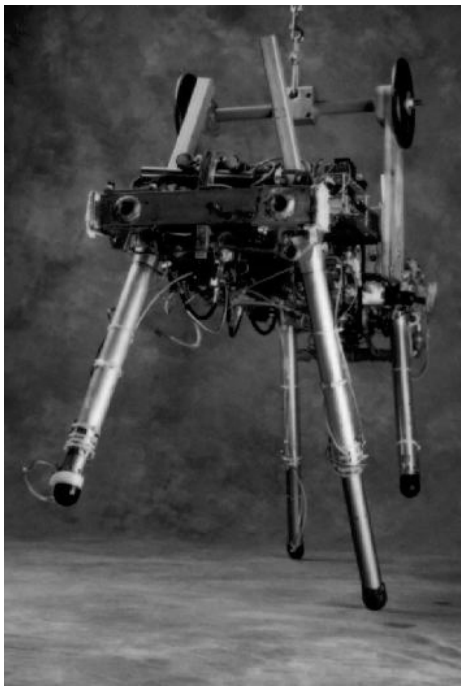

Figure 2.11: MIT Quadruped [54].

observed that 40 % of energy consumption during a stride was consumed by the hip actuator during the forward leg swing. By exploiting hip compliance and coordinating the vertical and rotational dynamics of the body, Monopod II (see figure 2.13) reduced the power consumed during locomotion from 125 W, for Monopod I, to less than 68 W of mechanical power [1, 2]. Both Monopods I and II used modified versions of the Raibert three part algorithm, for control of running. Ahmadi also proposed the non-dimensional *locomotion time* variable as a alternative means of parametrising locomotion behaviour.

More recently, Papadopoulos and Buehler [48, 49] showed that with a modified version of the three-part algorithm, simple torque control in stance, and a quasi-static slip control algorithm, stable pronking and bounding could be obtained despite a robot design that did not include linear leg actuation. Experimentation revealed open-loop stability of Scout II in running and proved robust to disturbances at speeds of up to approximately 1.2 m/s.

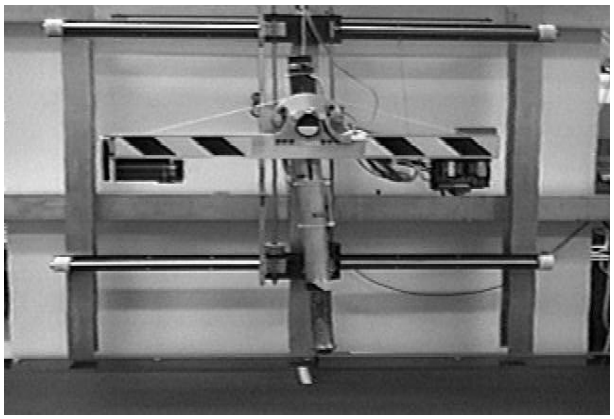

Figure 2.12: ARL Monopod I.

2.4.2 Control of Walking Robots with Articulated Legs

Since most legged robot designs are at least partially inspired by existing biological systems, it is natural to have develop control approaches for legged robots having articulated joints. Knees allow robots to more easily avoid toe stubbing, allowing repeatable cycles of support and leg swinging and to actively control robot torso height.

In the area of control development for such robots, Dunn and Howe [19, 20] proposed a dynamic bipedal walking controller that constrained touchdown hip velocity. Forward velocity tracking as well as step length control, two highly desirable characteristics for planning locomotion through unstructured environments, were achievable using this approach. Similar biped controls have also been published in the literature [18].

Virtual Model Control

Motivated by the difficulties of describing complex motion control tasks and the lack of formal control techniques for legged robots, Pratt [50, 35] proposed a control concept, called *Virtual Model Control*. This technique, which involves a forward kinematic analysis of the system, is based on using simulated virtual mechanical components, such as imaginary spring damper systems, to

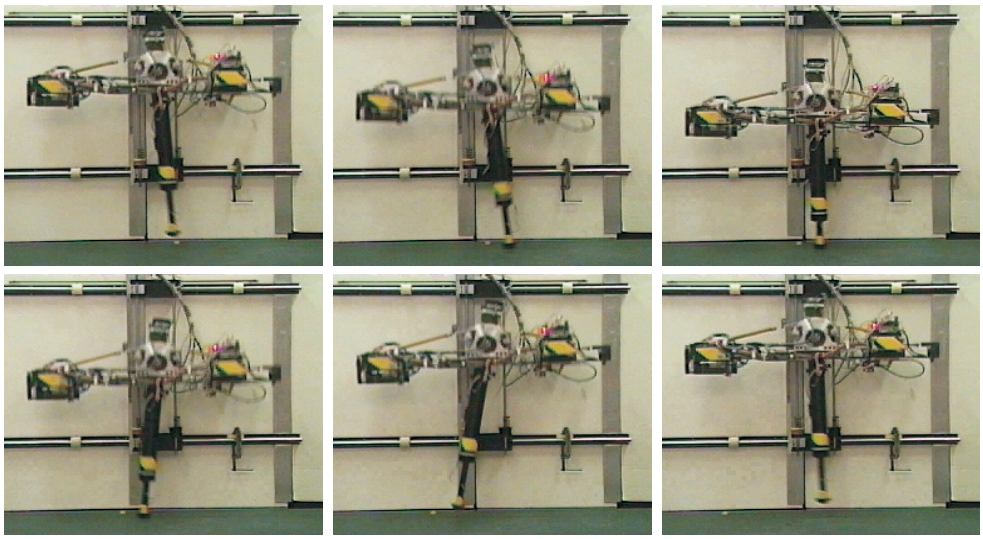

Figure 2.13: ARL Monopod II.

artificially constrain a system's bodies. By calculating the imaginary forces exerted on the system by the virtual components and by performing the appropriate transformations, torques and forces to command to real actuators can be calculated.

In addition to having a compact notation, virtual model control benefits from limited computational requirements since many of the key matrices may be precomputed and optimised. Furthermore, with the exception of parallel link systems, no matrix inversion is required. Lastly since virtual components are linearly additive, they may be easily superposed to obtained the combined effect of various virtual components. However, this approach still requires much control insight and manual parameter tuning in order to achieve the desired behaviour.

To date, the method has been applied to control several bipedal walking robots at the MIT Leg Lab including Spring Turkey [35] and Spring Flamingo [52] (see figure 2.14). Chew [12] later investigated the application of this technique to bipedal walking over sloped terrain. The method was also used in simulation on a hexapod robot that actively balanced an inverted pendulum on its back while walking using an alternating tripod gait [53]. Figure 2.15

shows the simulated hexapod.

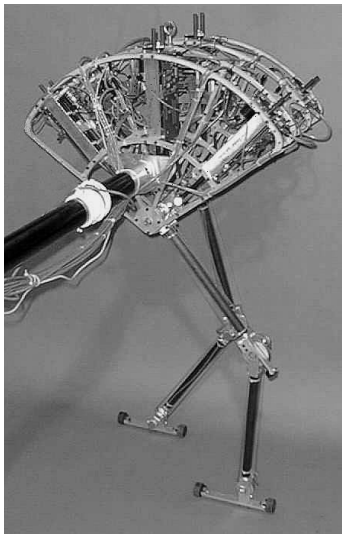

Figure 2.14: MIT Spring Flamingo.

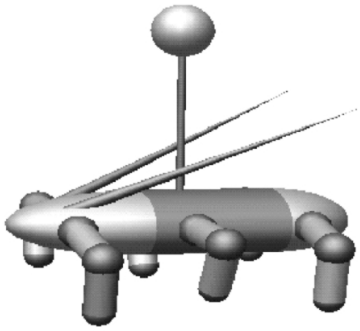

Figure 2.15: Simulated hexapod used to study virtual model control [53].

Zero Moment Point

Since foot rotation is a major cause of postural instability in dynamic bipedal locomotion, control strategies have been designed to deal with this unwanted phenomenon. One approach to solve this problem is to use a biped robot design having only point feet or alternatively by not applying ankle torque during periods of single support. Since it is advantageous to have feet for static stability and given that it is overly conservative to not apply any ankle torque during stance, researchers have often turned towards the concept of *zero moment point* (ZMP) for a more realistic estimate of the allowable bipedal walking stance ankle torque.

The idea of ZMP was first proposed by Vukobratović in 1969 [63] and since that time has been successfully used by a number of researchers, including most recently on the Honda humanoid robot [32] (see figure 2.16). According to Goswami [26, 25], who recently conducted a literature survey of ZMP research, the ZMP, or *center of pressure* CP as it is sometimes called, is

best defined as the point on the ground where the resultant ground reaction force *actually acts*. If the ZMP coincides with the location of the resultant force generated from the inertia and static gravitational forces acting on the system, there will be no moment acting on the body in the transverse direction. In reality the term ZMP is a misnomer, since only two of the three moment components tend to be zero, if the ZMP coincides with the point of action of the resultant body force. A moment is still usually produced by tangential ground friction forces acting about the central axis of the body.

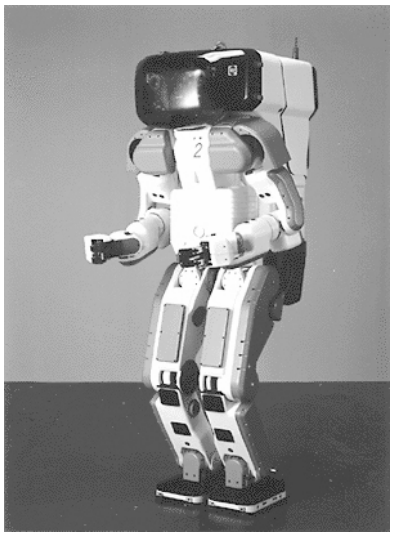

Figure 2.16: Honda humanoid robot [32].

The ZMP should not be confused with the *ground projection of the center of mass* (GCM) used in determining the stability margin of statically stable robots as mentioned in section 2. Figure 2.17 shows a simplified robot represented as a point mass supported by an actuated ankle. The left image of figure 2.17, shows the point mass hanging far to the right of the foot causing the GCM to lie outside the sole's area of support. If a torque is applied to counteract the static imbalance, the robot's ankle will rotate, effectively placing the ZMP at the toes. However, if the point mass is accelerated forward, as is the case of the right hand image of figure 2.17, the resultant force generated by the inertia and gravitational forces will place the ZMP under the foot thus avoiding tipping. A similar strategy of accelerating the heavy upper body of

the robot as a means of stabilising foot rotation was used by Hirai [32]. This is illustrated in figure 2.18.

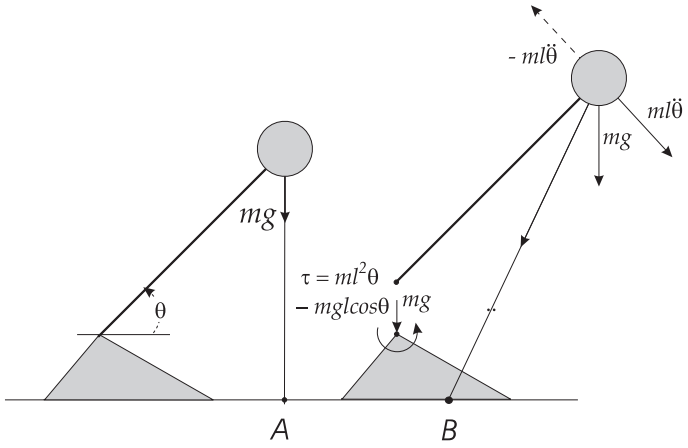

Figure 2.17: Foot and shank system. The leftmost figure will experience foot rotation if an ankle torque is applied. By accelerating the inverted pendulum forward, this can be avoided as shown in the rightmost figure (adapted from [26]).

Biomimetic Control Approaches

More biologically inspired methods of legged robot control have also been studied. Early research by Shik [58] pointed to a hierarchical structuring of the mammalian locomotory system, perhaps explaining the high degree of adaptability commonly observed in animals. By electrically stimulating the mid brain region of a De-cerebrated cat, Shik found the cat could be induced to walk. Varying input intensity affected both frequency and walking gait adopted.

Because of such experimental findings and the common observation that humans flexibly adapt to unpredictable environmental changes, it is often argued that a low level *central pattern generator* (CPG) must be responsible for the generation of locomotory behaviour in mammals, fish, and insects. This view of locomotory control, based on the neurophysiological findings of Grillner [29], sharply contrasts classical control theory. Rather than commanding

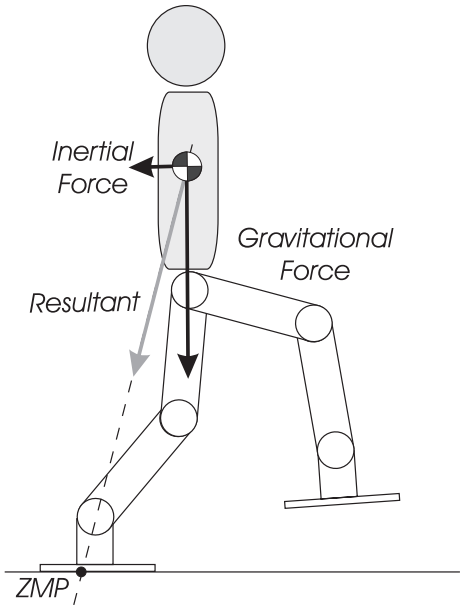

Figure 2.18: Planar biped model showing ZMP. By accelerating the heavy upper body, the resultant inertia and gravity force acts under the foot. If this point coincides with the ZMP moment will be induced on the robot's ankle (adapted from [32]).

joint trajectories and relying on feedback to provide real-time adaptability to the system against disturbances and errors, CPG based methods rely on the emergent behaviour stemming from interactions between the rhythmic activities of the neural system, the musculo-skeletal system, and the environment. The use of a hierarchical approach is also found in the work of Brooks [9], in the artificial intelligence community, who obtained complex robot behaviour using a layered *subsumption architecture*.

A commonly used CPG, based on modeling the neural physiological system of animals is the *neural oscillator* (NO). A NO consists of a network of neurons connected in such a way that one neuron's excitation suppresses that of the others. Due to these inhibitory connections, torques are induced in alternating directions corresponding to muscle flexion and extension. Although other neuronal network representations exist, the model proposed by Matsuoka [39] is often used in the context of biomimetic robot control. Equation 2.1 shows the mentioned model and an illustration is provided in figure 2.19.

In equation 2.1, u_i is membrane potential of the neuron body, τ is a time constant determining the rise time for a step input, β determines the steady state firing rate for a constant input, v_i is the adaptation variable, τ' is a time constant specifying the time lag before adaptation takes effect, and y_i is the neuron output. Feedback is also incorporated into the neural oscillator model, as can be seen from the presence of a feedback term in equation 2.1.

$$\begin{aligned} \tau \dot{u_i} &= -u_i - \beta v_i + u_0 + Feedback_i + \sum_{j=1}^{n} \omega_{ij} y_j \\ \tau' \dot{v_i} &= -v_i + y_i \\ y_i &= max(0, u_i) \end{aligned} \tag{2.1}$$

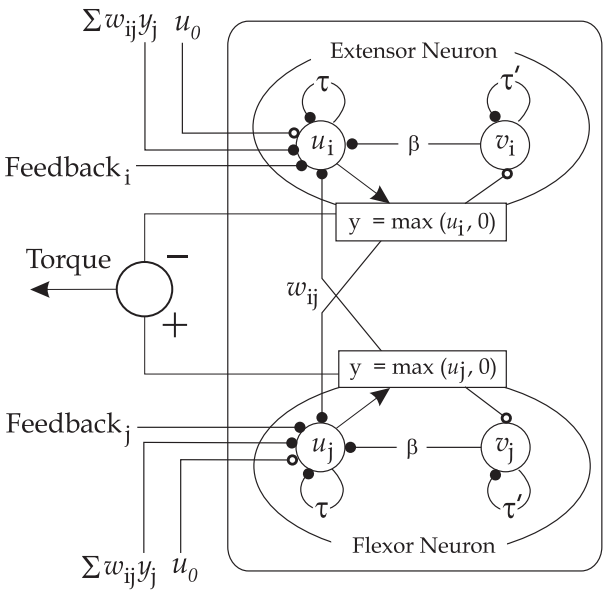

Figure 2.19: Neural oscillator model (adapted from [30]).

In addition to being the first neuronal network model to incorporate adaptation, the Matsuoka's model is of particular interest since it has been used by Taga [61, 60] to obtain planar bipedal walking in simulation and more recently by Kimura [30, 36] to obtain experimental walking and running results in a quadruped robot, Patrush. Kimura also added other biologically inspired layers to his walking controller.

Although NO methods of locomotion control are appealing because they aim to model nature, they are not without shortcomings. Firstly, our understanding of the mammalian neurophysiology is still limited, as is our knowledge of the neuronal circuits making up these organisms. This poses some significant problems since NO output varies significantly depending both on the number and weight of connections. Furthermore, given the strong interconnection in typical NO circuits, additional connections increase the parameter space exponentially, making the incremental addition of complexity prohibitive. NO output is also highly sensitive to parameter variations, with small modifications producing significantly different output. Although certain parameters are attributed with playing different roles in shaping output, considerable interdependency still exists. Since the parameter space is extremely large to begin, NO circuit tuning can easily become intractable. Lastly, the feedback mechanisms used by living organisms is still unknown, making the choice of a feedback expression for equation 2.1 somewhat arbitrary. Taga and Kimura both used knee joint angle as feedback in the hip NO.

2.4.3 Passive Dynamics in Legged Robot Control

Another area of research in legged robotics, is the study of mechanism design as a means of reducing mechanical complexity and energy consumption. By replacing motors with passive joints or springs, equivalent motions can be obtained without added power requirements. From a controls point of view this approach makes a lot of sense; If the passive (unforced) system response can be used as much as possible, required control actions can be minimised thereby reducing power consumption and potentially simplifying control.

The seminal work in this area was done by McGeer [40] who built a series of bipeds capable of walking passively down shallow inclines powered only by gravity. McGeer first studied a biped with rigid legs that used active foot retraction to ensure the swing foot cleared the ground (see figure 2.20). Subsequently, he conducted a parametric study of various physical parameters such as foot radius, leg inertia, center of mass location, and hip mass to

determine their impact on walking. This work was later followed by the study of a experimental biped having passive knees [41]. These mechanisms were shown to be passively stable and robust to minor perturbations. Garcia, Chatterjee, and Ruina [24] later expanded upon McGeer's analytical findings, stating necessary conditions for optimal walking efficiency.

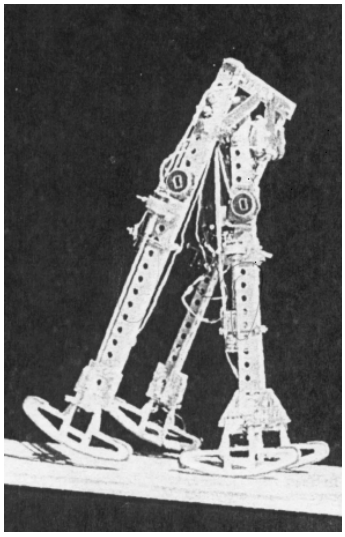

Figure 2.20: McGeer's gravity powered passive walker without knees [40].

The ideas proposed by McGeer have also been used as the basis of control for legged robots with actuated joints. In this area, Pratt [51] reversed the knees of the spring flamingo biped (see figure 2.14) to allow the knee joint to act almost entirely passively during swing thus significantly reducing energy consumption. Hawker amd Buehler [31] applied a similar strategy to control the lower leg motion of a version of the Scout II quadruped with knees. The leg design used a completely passive knee that could be locked/unlocked using a solenoid. This approach, permitted planar quadrupedal trotting. To eliminate roll instabilities resulting from the planar leg design, the robot was constrained to only move in the saggital plane.

Related research has focused on exploiting robot design to passively stabilise running of legged robots. Ringrose [57] showed that using (roughly) semi-circular feet for a series of monopods, bipeds, and quadrupeds stable dynamic running could be achieved without any sensory feedback. His findings

suggested that it would be possible to build robots containing no sensors, by carefully designing the robot's mechanical system.

Similarly, Buehler, Cocosco and Yamazaki [10, 11] showed that using a simple robot design having only one actuated degree of freedom per joint, stable open-loop walking, turning, and step climbing could be achieved despite using only limited feedback. Their Scout I and Scout II robots, used stiff stick legs and relied on momentum transfer to maintain regular body pitching. A simple *ramp controller* was proposed that used a four state state-machine, based on the overall robot state, to coordinate locomotion activities. These four phases were 1) Front support, 2) Front to back double support, 3) Back support, 4) Back to Front double support. Figure 2.21 shows Scout II (with stiff legs) in these four phases of motion.

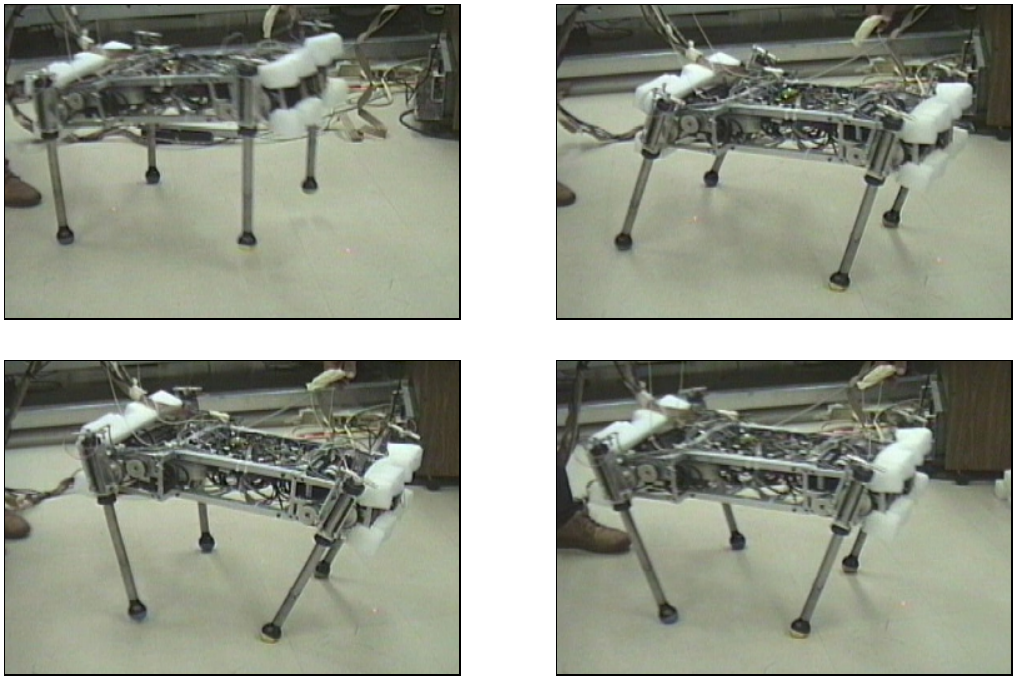

Figure 2.21: Scout II walking with stiff legs. Images are read left to right, top to bottom.

Figure 2.22 shows the devised ramp control. As illustrated, when the robot entered the back leg support state, the back legs were swept at a constant rate $\dot{\phi}_2$, between a fixed touchdown angle $\phi_{2\,start}$, until the front legs entered a

support phase. Here ϕ is the leg angle with respect to the body. The legs were then kept at a their touchdown position $\phi_{2\,end}$ for a fixed period of time, before being retracted back to their touchdown position. Throughout this process, the front legs where kept "locked" at a perpendicular position with respect to the body.

The ramp controller was open loop and only needed to know if the legs were in contact with the ground. Thus since only limited proprioceptive sensing was required for the controller it was extremely straightforward to implement. Using numerical analysis of Scout's equations of motion, Cocosco [13] showed a nearly global domain of stability for the controller, even though no active stabilisation was being used.

Although the controller showed a great deal of promise and was very successful on Scout I, leg impacts during stiff legged walking were quite significant on Scout II. These large impulsive forces resulted in undesirable stressing of the robots mechanical system and in lossy dynamics. These factors motivated the use of compliant legs on Scout. It was believed that adding compliance in the legs, would also permit previously unrealisable running gaits such as the bound.

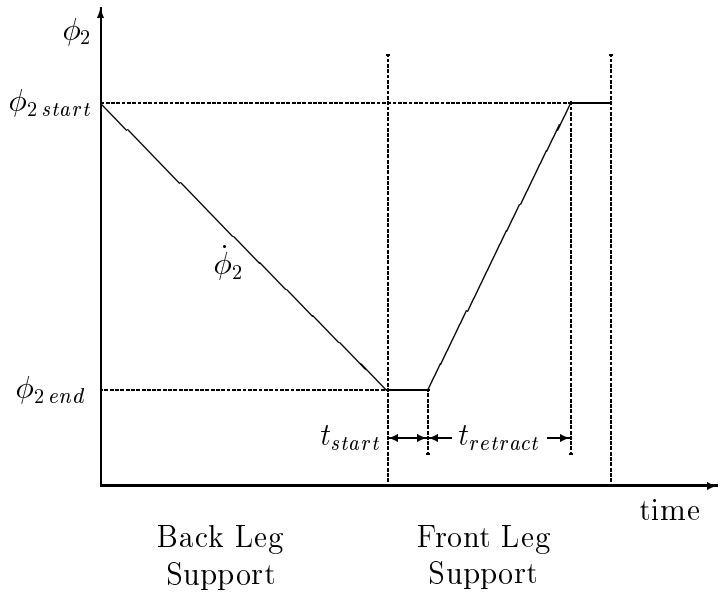

Figure 2.22: Ramp controller input for ϕ_2 for one complete step.

2.5 Summary

This chapter presented an overview of animal gaits aimed at familiarising the reader with relevant terminology needed in future discussion. Although no work exists on dynamic walking controller design for underactuated quadruped robots, research was described in three closely related areas: control of dynamic running robots, control of dynamic walking robots with articulated legs, and exploiting passive dynamics in legged robot control.

Chapter 3

Scout II

3.1 Overview

This chapter describes the Scout II robot, for which the control algorithms discussed in thesis were developed. Mechanical, electrical, and software specifications for the system are discussed. In addition, motivation and design decisions used in the redesign of Scout's electrical and software systems are described.

3.2 Platform Specifications

The locomotion algorithms developed for this thesis, were designed for the Scout II robot. Scout II is a quadruped robot developed at McGill University's Ambulatory Robotics Lab (ARL) by Robert Battaglia [6] with the aim of investigating the feasibility and trade-offs of underactuation in legged robots.

3.2.1 Mechanical Subsystem

Each of Scout II's legs has one actuated rotational hip joint and a passive prismatic joint. The prismatic legs joints can be locked for stiff legged operation or used in a compliant mode. When used in the compliant mode, the leg design can accommodate a wide range of springs, allowing the system dynamics to be tailored to the desired response. Similarly, the robot's leg length can also be modified using various leg extenders. Figures 3.1 - 3.3 show pictures of Scout II. For clarity, relevant robot parameters have been summarised in table 3.1.

All experiments documented in this thesis used two springs on each of Scout's legs to obtain the desired leg stiffness. This resulted in a leg spring stiffness of approximately 2250 N/m. This leg stiffness was chosen experimentally since lower spring constants produced sluggish or undesirable body behaviour. The chosen spring combination also allowed a single leg configuration to be used for both running and bounding. A detailed description of the springs used during experiments is provided in table 3.2. For simplicity, the robot leg length was not altered.

Since Scout II was designed to operate without a tether in unstructured urban environments, all computing, sensing, and power subsystems are contained on board the robot. To date, the mechanical design has proven quite rugged and has endured considerable abuse from continuous experimentation. Unfortunately the electrical subsystem did not show the same resilience and thus a complete redesign of this system was undertaken as part of this thesis. Furthermore, since considerable coupling existed between the electrical system and the implementation of the real-time software architecture used to control the robot, the software subsystem was also redesigned and implemented. Sections 3.2.2 and 3.2.3 describe design considerations and implementation decisions taken as part of this process.

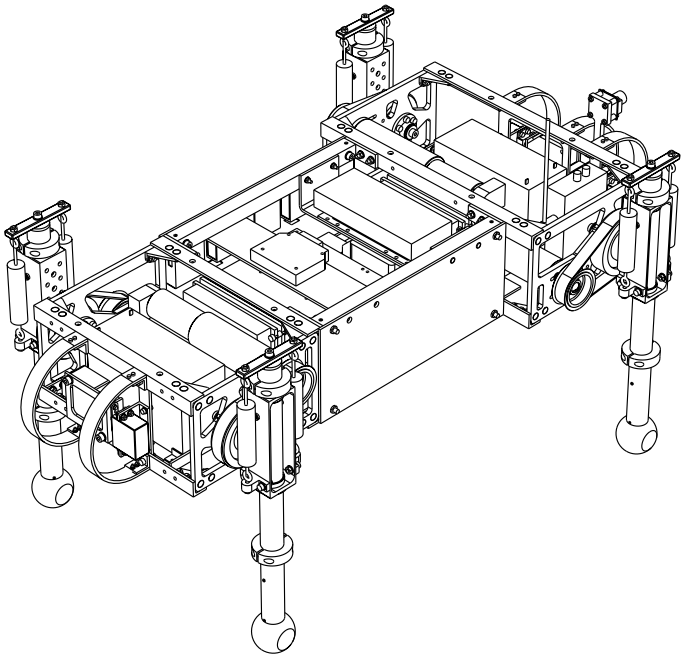

Figure 3.1: Pro/Engineer rendering of Scout II with linear compliant Legs.

3.2.2 Electrical Subsystem

A robot such as Scout II, that is used as a research platform, must simultaneously fulfill many unique requirements that do not make a highly embedded hardware approach desirable. Although the entire electrical subsystem could be tightly integrated onto a custom circuit board, with all computing handled by a modest microprocessor, this approach would prove too restrictive in the long run. Since the robot is continuously being modified and improved, the chosen electrical hardware must lend itself to the rapid integration of new sensors as well as to the quick implementation and debugging of new locomotion controllers. Furthermore, since interactions between the robot and the environment are not always visually apparent, the system must also have a flexible data logging system allowing users to easily store run time data for off line analysis.

As shown in figure 3.4, the electrical system can be divided into 3 major subunits : the power distribution, the data acquisition, and the comput-

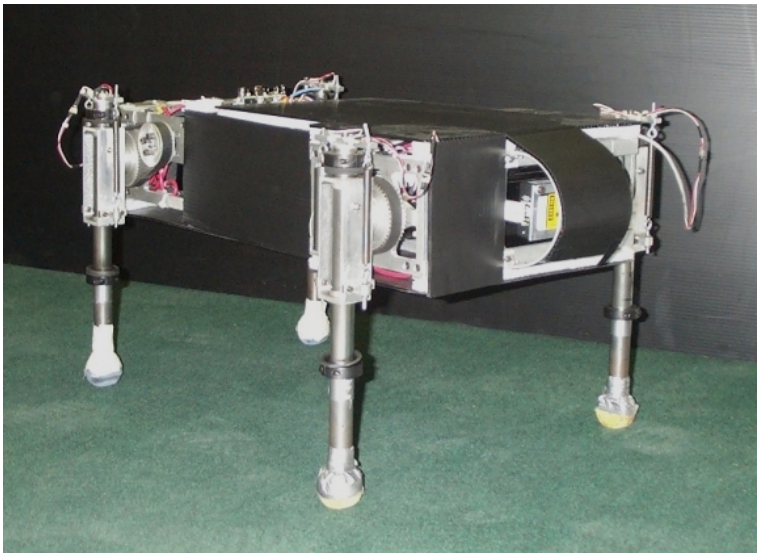

Figure 3.2: Scout II with linear compliant legs

ing/control subsystems.

The first iteration of Scout II's electrical system used a custom data acquisition system developed at ARL by Nadim El-Fata called the *Standard Parallel Port/Serial Peripheral Interface* (SPP/SPI) system. The SPP/SPI system is a distributed data acquisition system that uses the computer's parallel port and the serial peripheral interface (SPI) communications standard to perform input/output (I/O) with up to 8 input and 8 output custom data modules at rates of up to 1 kHz. At the heart of the SPP/SPI was a multiplexer board that plugged into the computer's parallel port and interfaced to various I/O modules. This multiplexer had telephone style connectors allowing users to rapidly customise the system to their particular sensing requirements. Figure 3.5 shows a photograph of the SPP/SPI system as it used to be mounted on Scout. Scout II used two SPP/SPIs.

Although use of the SPP/SPI was extremely successful on Scout I [64], since the robot used only limited sensing, it did not scale well to the larger Scout II robot. Because of its distributed architecture, a system such as the SPP/SPI significantly increased the amount of cabling on the robot, leading to frequent loosening and breaking of cables. In addition, the added power re-

Table 3.1: Scout II mechanical specifications [6]. * The reported overall robot mass was calculated after the electrical system redesign.

Parameter	**Value**	
Body length	0.837 m	
Body height	0.126 m	
Front hip width	0.498 m	
Rear hip width	0.413 m	
Hip-to-hip length	0.552 m	
Total mass*	25.545 kg	
Body mass	21.865 kg	
Body Inertia from COM about		
pitch axis	1.091 $kg\,m^2$	
roll axis	0.161 $kg\,m^2$	
Leg length	0.255-0.457 m	
Leg mass	0.920 kg	
Leg inertia (about hip)	Length (mm)	Inertia ($g\,mm^2$)
	255.9	12.94
	275.0	14.27
	294.1	16.26
	313.2	18.90
	332.3	22.19

quirements resulting from distributing computing to individual data modules, proved to be ill suited for a mobile robot such as Scout II.

The mentioned shortcomings of the SPP/SPI motivated a shift to a centralised data acquisition system using standard off the shelf components, capable of meeting Scout's present and future needs. Given the need to change the data acquisition system, the opportunity was also taken to upgrade the robot's computer. A discussion of the chosen architecture and of the designed custom electronics follows.

Table 3.2: Springs used on Scout II for thesis experiments. For more details refer to [34].

SPEC Cat. No.	**Stiffness** (N/m)	**Pretension** (N)	**Max Extension** (m)
E0750-095-4500	2170.0	16.50	0.19075
E0360-055-4000	78.3	7.12	0.15494
Total	2248.3		

Computing and Data Acquisition Architecture

To ensure robust future operation of Scout II, the SPP/SPI system was replaced by an PC104 computer system. PC104 [15] is a standard for industrial and military grade embedded computers. Since all PC104 modules are designed with the same physical dimensions and use a standardised bus connector, computing, storage, and data acquisition capabilities of a computer can be customised to meet the needs of a particular application. Selected components are then stacked on top of one another like LEGO bricks to form a custom computer configuration. The small footprint of this standard makes it ideally suited for mobile robotics applications where space is often at a premium. Furthermore, by using a shared bus connector and few external wires, wiring breaks and bends can be minimised. In total, seven PC104 boards were selected for Scout. Table 3.3 summarises the PC104 modules selected following a search of PC104 vendors. Key features of each module are also listed. Figure 3.6 shows a picture of the PC104 stack mounted on the robot.

Since the PC104 data acquisition modules (i.e. DM6814 and MPC550) used large multi-pin headers to provide access to their functional blocks, two custom interface boards needed to be designed. These printed circuit boards provided a convenient and uniform interface to which sensors could be connected. In addition, to make use of the full range of the analog to digital conversion (ADC) hardware on the MPC550 card, scaling, buffering, and anti-

aliasing circuitry needed to be designed. Table 3.4 summarises Scout's I/O needs, classifying items according to the required type of I/O. Appendix A contains all the schematics for the designed custom hardware.

3.2.3 Software Subsystem

Previous designs and implementations of the software subsystem for Scout did little to abstract out specifics of the hardware operation from the state based runtime robot code. In addition, the software subsystem, which was mainly legacy code from previous projects, contained many inconsistencies. These and other points strongly motivated a redesign of the software subsystem to limit coupling and to improve overall system performance.

Although the data logging system from the original Scout code was maintained, given its ease of use, the remainder of the code was revised to eliminate all assumptions regarding the data acquisition hardware. By abstracting out the specifics of the low-level hardware it was ensured that future modifications of Scout's physical hardware would not interfere with the higher level state based control code.

Control Code Architecture

As in the past, Scout II used the QNX realtime operating system (OS) [38]. QNX is a POSIX compliant multi-process, multi-user UNIX flavoured real-time OS. Although QNX supports multiple processor, and uses a preemptive priority based scheduler to ensure all processes are properly serviced, the kernel is not thread safe. Therefore, although multiple processes can be run, users must resort to interprocess communication or message passing schemes to allow processes to share information. Since interprocess communication can be a costly approach to sharing data, degrading performance, the code was instead designed using a simple polling scheme. Using this scheme, data was gathered, computation was performed, to determine state variables, and

output commands were sent to the actuators at each execution loop.

To modularise some additional functionality, a few blocking processes were implemented that took care of some low bandwidth activities, such as waiting for instructions from a TV remote infrared module that was connected to one of the computer's serial ports. This allowed users of the robot to send high-level instructions or to dynamically vary parameters during experiments.

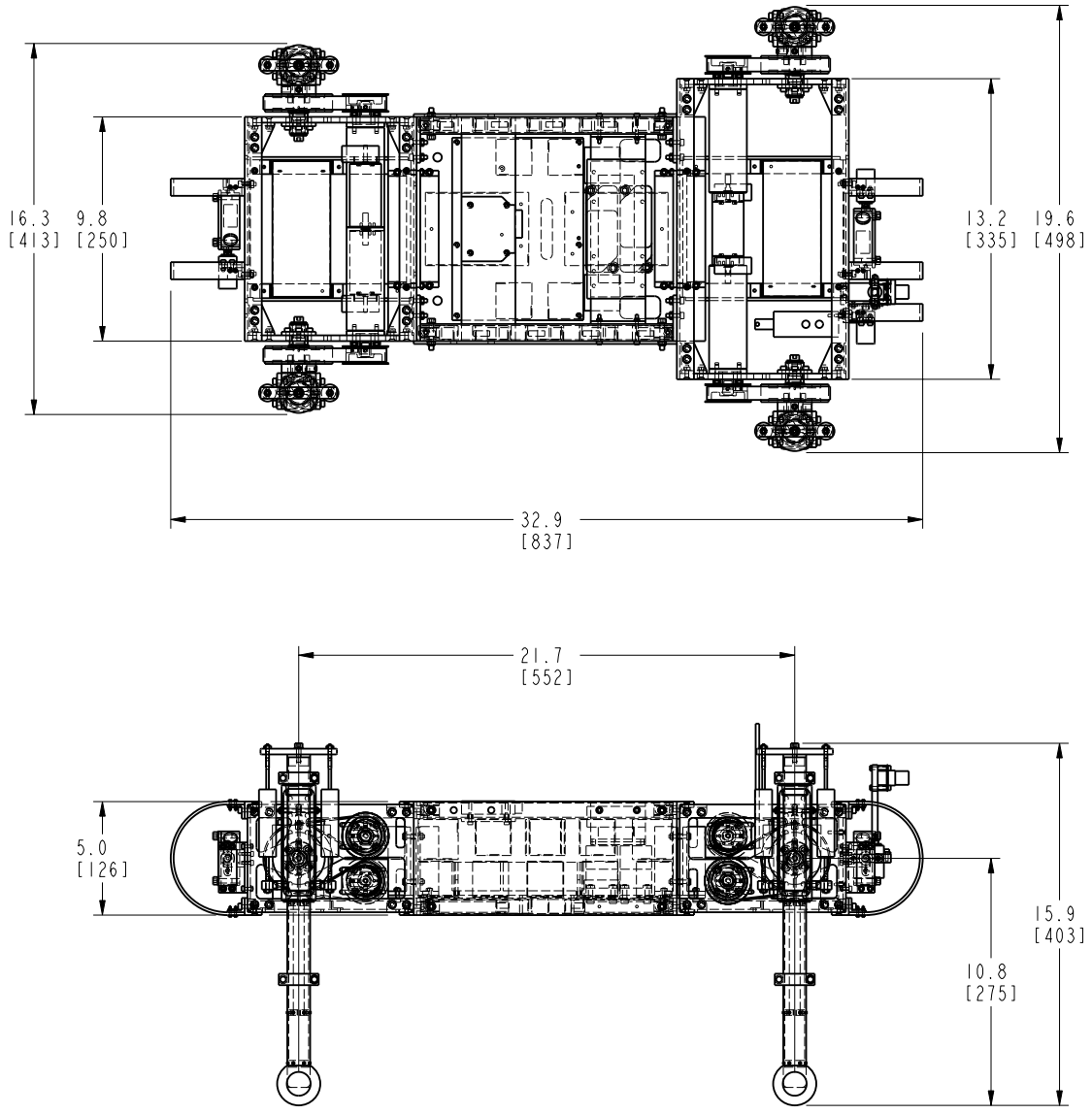

Figure 3.3: Top and side Pro/Engineer isometric views of Scout II.

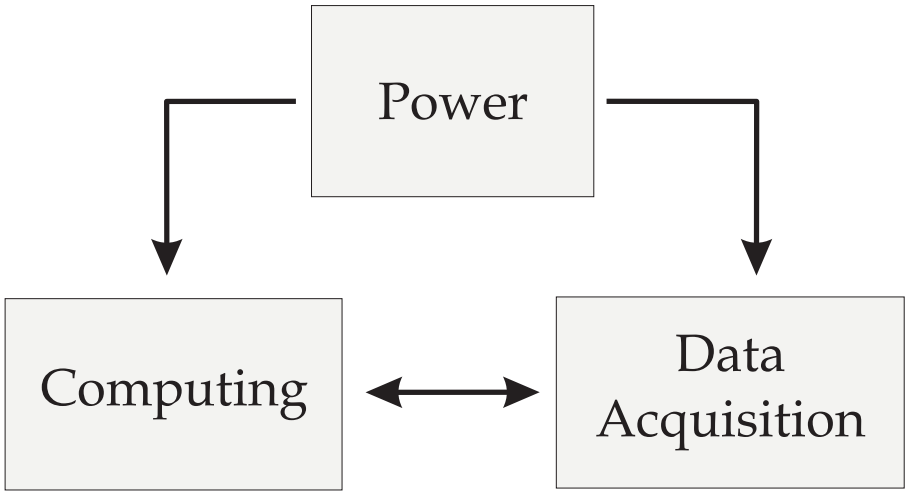

Figure 3.4: Electrical system block diagram. This system can be subdivided into three main subsystems : power distribution, computing and data acquisition.

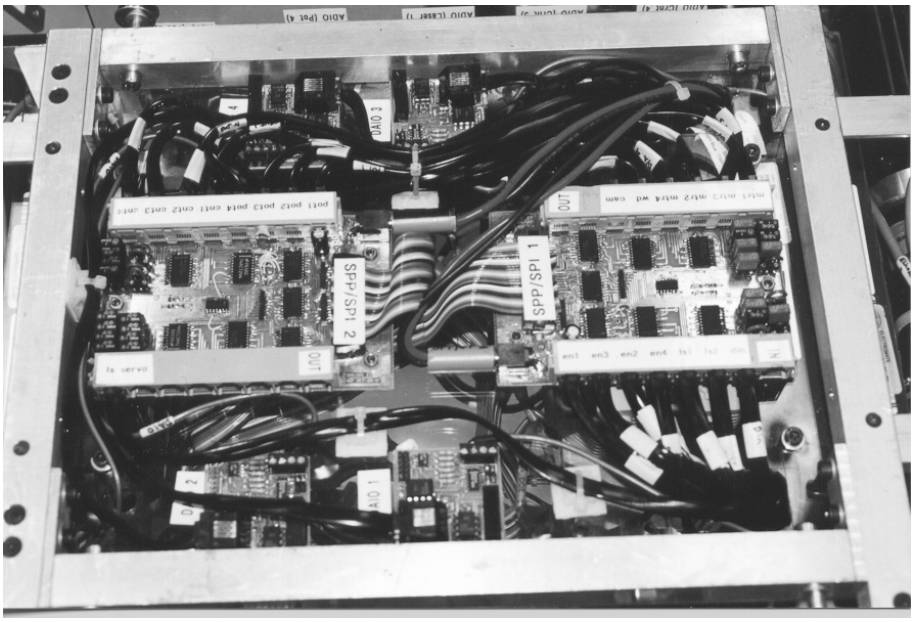

Figure 3.5: Underside of Scout, showing SPP/SPI multiplexers and connected data I/O modules.

Figure 3.6: PC104 computer mounted inside robot chassis. Designed custom I/O boards can be seen on left hand side of image.

Table 3.3: PC104 modules selected for Scout II following web search of hardware vendors

Part No.	**Quantity**	**Description/Features**
CMW6686GX233-64/DO16	1	- Pentium 233 MHz CPU Module - SVGA controller - 2 RS232 serial ports - 1 ECP/EPP parallel port - Keyboard interface - 64 MB RAM with 16 MB Flash Disk
EPWR104	1	- 50W Power Supply Module. - Input Range : 8-40 VDC - Output Range : +5 VDC @ 5 A +12 VDC @ 2 A −12 VDC @ 0.5 A
CM202	1	- PC104 Networking Module - NE-2000 Ethernet with AUI - 10Base-T and 10Base-2 interfaces
CMT107	1	- 6GB IDE Hard drive Module - IDE Controller and slave connector
DM6814	2	- 3 16-bit incremental encoder channels - Digital (6 bi-directional, 12 input) - 3 16-bit counter/timers (8 MHz)
MPC550	1	- 16 12-bit analog inputs - 24 digital I/O lines - 8 12-bit analog output channels - 3 16-bit counter/timers (7 MHz)

Table 3.4: Scout II I/O requirements

Direction	Type		Quantity
INPUTS	**ANALOG**		
	Leg Pots	4	12
	Lasers	2	
	Gyroscopes	1	
	Battery Voltage	1	
	Battery Current	1	
	Applied Torque	4	
	DIGITAL		
	Hall Effect Sensors	4	4
	HCTL		
	Optical Encoders	4	4
	Total		20
OUTPUTS	**ANALOG**		
	Commanded Torque	8	8
	DIGITAL		
	Watchdog	1	1
	PWM		
	Servos	2	2
	Total		11

3.3 Summary

This chapter presented a description of the experimental hardware platform, the Scout II robot, for which locomotion algorithms were developed. An overview of key robot subsystems and of design decisions used in the overhaul of the robot's electrical system was also presented. Lastly software design and implementation issues relating to the robot's realtime control code were also addressed.

Chapter 4

Modeling

4.1 Overview

A review of currently available locomotion controller design tools for highly non-linear and underactuated systems such as Scout II reveals that no adequate theory or techniques exist at this time. Therefore, the synthesis of new locomotion controllers relies principally on the development of intuition, by the controller's designer, about system behaviour and dynamics. To help in developing this intuition, we have found that an iterative process of simulation and analysis is a good approach.

This section presents modeling and simulation results used to investigate walking. It was hoped that by using simulation, intuition could be developed to help guide the design of a walking controller. To begin, a rocking controller was designed and simulated, that excited the body at its natural frequency and repeatedly lifted fore and hind legs off the ground. This controller proved robust to large variations in parameters even though it was completely open loop. Next, the rocking controller was modified to obtain stable open loop walking. Minor modification to the walking algorithm allowed open-loop velocity tracking.

4.2 Simulation Package

To perform the simulations for this thesis, the Knowledge Revolution *Working Model 2D* (WM2D) package was used [56]. WM2D, a graphical physics simulator, allows the simulation of multiply linked planar rigid bodies under a number of user specified constraints and inputs.

One of the big advantages of using a package such as WM2D is that it does not require the derivation of the system equations of motion. Instead, systems can be interactively built and simulated, using a straightforward object-oriented scripting language. WM2D uses a fifth order Runge-Kutta integrator that numerically integrates the effects of all the forces acting on the bodies being simulated, yielding accelerations, velocities, and position information. As with any numerical technique, small errors can add up over time, producing incorrect results, therefore, an adaptive time step is used by the program to bound errors at each time interval.

Using this package, a simulation model of Scout II was constructed having the same geometric and mass/inertia parameters as the real robot (see table 3.1). Figure 4.1 shows this model. The constructed model consisted of seven rigid bodies: top and bottom leg sections and a circular toe for each leg, as well as a main torso. To model the robot's passive prismatic leg joint, the top leg section was constrained to move along a frictionless slot placed in the lower leg. A spring/damper system was also connected between these bodies to provide the correct compliance. Each leg was then attached to the main torso via a torque mode actuator. To prevent excessive spring extensions and to properly model Scout's real legs, two ideal ropes (i.e. no stretch) were also connected between top and bottom leg sections. The ropes modeled leg clamps on the robot that limited leg compression.

In addition to physical parameters obtained directly from the robot, certain other parameters had to be estimated. These values are summarised in table 4.1. Some of these parameters such as viscous damping c and floor Coulomb friction μ_{floor} were selected based on prior attempts to match simu-

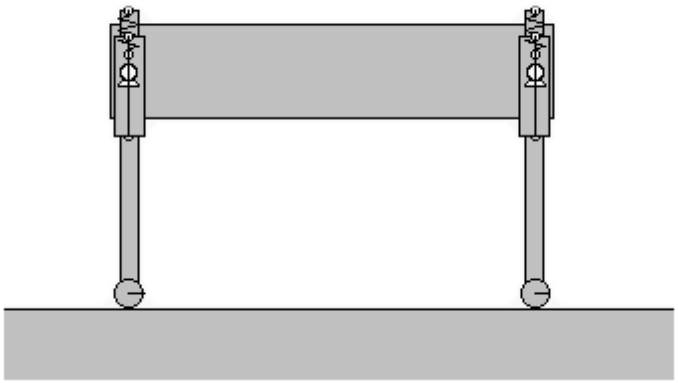

Figure 4.1: Working Model 2D Scout model

lation behaviour to experiment by Battaglia [6], Papadopoulos [48], and Yamazaki [64].

Table 4.1: Working Model 2D simulation parameters

Parameter		Value
Physical	viscous damping (c)	60 Ns/m
	toe elasticity (ϵ_{toe})	0.8
	floor friction (μ_{floor})	0.8
	floor elasticity (ϵ_{floor})	0.2
Integrator	animation step	0.0015 s
	overlap error	0.001 m
	integrator error	0.00001

4.3 Rocking

Since Scout II does not have knees, one of the major obstacles to overcome in designing a walking controller is to find a means of reliably moving the robot from rest to steady state oscillatory behaviour. Once the robot is pitching regularly, the task of designing a walking controller is considerably simpli-

fied, since the system will have a tendency to passively maintain this rocking motion.

When the robot is at rest, there is a 0^o phase difference between the front and back sets of legs. This is also true in rocking, with the additional characteristic that legs also alternate repeatably between stance and flight. Therefore, rocking was first studied as a means of providing a reliable startup sequence for a robot walking algorithm. It was envisioned that by having alternating periods of stance and flight at regular intervals that the rocking controller could later be modified to produce a stable walking gait. A similar strategy was used by Kimura [30] to excite Patrush, a quadruped robot with knees, from rest to a running bound, via an intermediate hopping state.

4.3.1 Rocking Model

To study the natural dynamical behaviour of the robot, a simplified planar two-dimensional robot model was derived and analysed. Figure 4.2 shows this model. Scout II is modeled as a planar spring mass damper system with massless legs.

Instead of lumping the robot's overall mass at the geometric center of the torso, the presented model split the overall mass into two point masses (each having half the robots mass) located at a distance r (i.e. the radius of gyration) from the center of the body. According to Beer and Johnston [7], the radius of gyration is the distance at which the mass of a body should be concentrated if its moment of inertia with respect to some rotational axis is to remain unchanged.

$$r = \sqrt{\frac{I}{M/2}} = \sqrt{\frac{1.091}{12.5}}\, m \; = \; 0.295\, m \tag{4.1}$$

Equation 4.1 shows the calculated value for the radius of gyration based on Scout II's current physical parameters. This value is very close to the value

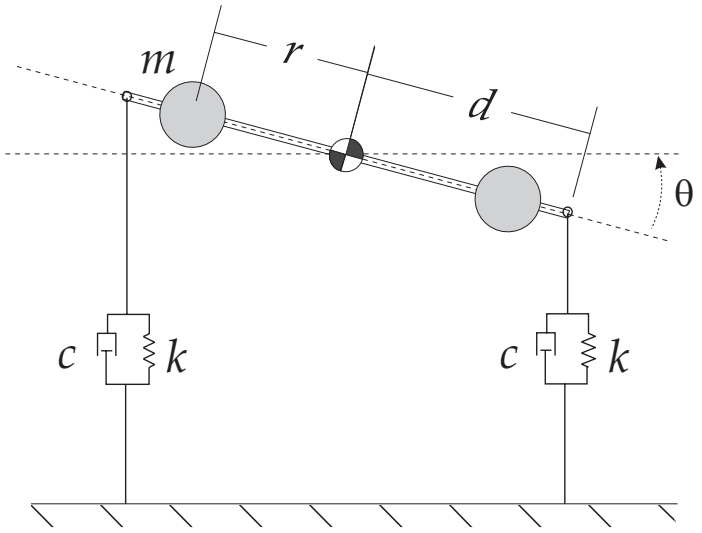

Figure 4.2: Simplified rocking robot model - d is half the leg separation (m), r is the radius of gyration (m), m is the half the body mass, c is the damping constant (Ns/m), and k is the linear leg spring constant (N/m).

of half the hip separation length d (i.e. $0.276\,m$). Thus, we can think of the model of figure 4.2 as two single leg models (shown in figure 4.3). Assuming small body oscillations, analysis can thus be conducted on the single leg model, treating eventual coupling effects between legs as system disturbances. This is analogous to the approach used by Raibert in formulating his three part control law (see section 2.4.1). Thus, analysis of the planar robot model of figure 4.2 simplifies to the analysis of a classical spring mass damper system (see figure 4.3).

Given this simple model for the dynamics of a leg, the next step was to extract a meaningful parameter to be used in the design of a rocking controller design. From vibration analysis [62], it is known that if a system is excited at, or near, its natural frequency

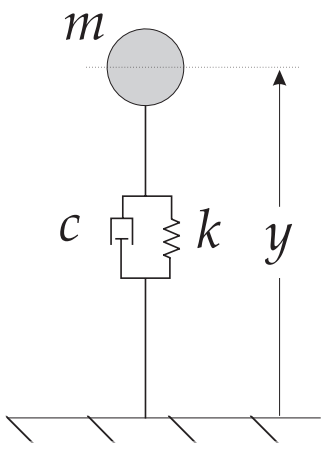

Figure 4.3: Single leg robot model - m is half the total robot mass (kg), y is the height of the point mass measured from the ground at a particular instant of time, k is the linear leg spring constant, and c is the damping constant.

$$\omega_n \;=\; \sqrt{\frac{k}{m}} \;=\; \sqrt{\frac{3050}{12.5}}\ rad/s \;=\; 15.6\ rad/s \tag{4.2}$$

it will begin to resonate. Considering damping, the resonant frequency is

$$\begin{aligned} \omega_d \;&=\; \omega_n\sqrt{1-\zeta^2} = \omega_n\sqrt{1-\left(\frac{c}{2\sqrt{k\,m}}\right)^2} \\ &=\; 15.6\ \sqrt{1-\left(\frac{60}{2\sqrt{3050\cdot 12.5}}\right)^2}\ rad/s \;=\; 15.23\ rad/s \end{aligned} \tag{4.3}$$

Although the spring stiffness value used in the above equations is less than the stiffness of springs later selected for the real robot (see section 3.2.1), these value were originally chosen since they yielded the lowest body rotational frequency while still allowing repeatable steady state rocking.

Using the above calculated natural frequency, a simple rocking controller was devised, that excited the system at this frequency. This controller and results from simulations of the controller are discussed in section 4.3.2.

4.3.2 Open Loop Rocking Controller

Once the natural frequency of oscillation for the single leg model had been calculated, a stable rocking controller was designed around this parameter. Sinusoidal γ and cosinal $\dot{\gamma}$ trajectories were commanded, at the calculated natural frequency of the single leg model. Once the leg trajectories had been determined, using equations 4.4 and 4.5, a *proportional derivate* (PD) controller was used to command the correct torque to the hip motors (see equation 4.6). Simulation PD controller gains were set to $\kappa_p = 50\ Nm/deg$ $[0.872\ Nm/rad]$ and $\kappa_v = 1\ Nms/deg$ $[0.0262\ Nms/rad]$. In equations 4.4 - 4.6, i stands for either the front or back sets of legs. For reference purposes, all equation parameters are shown in figure 4.4.

$$\gamma_{i\,d} = A\sin(\omega_n t) \tag{4.4}$$

$$\dot{\gamma}_{i\,d} = A\,\omega_n\,\cos(\omega_n t) \tag{4.5}$$

$$\tau_i = \kappa_p\,(\gamma_i - \gamma_{i\,d}) - \kappa_v\,(\dot{\gamma}_i - \dot{\gamma}_{i\,d}) \tag{4.6}$$

As previously mentioned in section 1.3, given the range of operation of Scout's actuation, achievable torque is highly dependent on shaft velocity. Thus to ensure that this relationship was correctly modeled and that commanded simulation torque matched realistically achievable values, a motor torque/speed model was implemented as part of the simulation. Figure 4.5 shows the motor limits specified by the torque/speed curve for the first quadrant of motor operation (i.e. positive torque and velocity). Since the configuration of Scout's actuation system can be modified to select different sprocket combinations, graphs are provided for both currently used combinations. All simulations documented in this thesis used the 48/34 torque/speed motor characteristics shown in figure 4.5b. The mentioned torque/speed characteristics have been experimentally verified via motor dynamometer tests, documented by Battaglia in [6]. Using the described controller, with a trajectory amplitude A of 3.5^o, stable rocking was obtained. Section 4.3.3 discusses

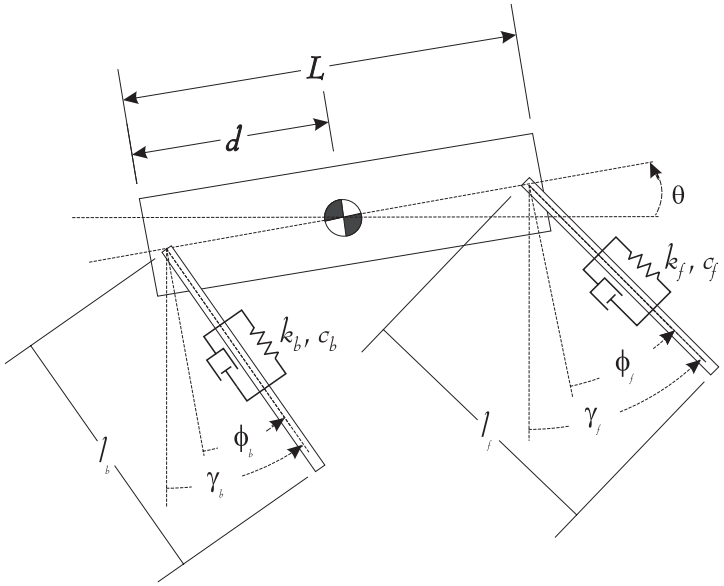

Figure 4.4: Planar model of scout, showing chosen nomenclature.

these results.

4.3.3 Simulation Results

Figures 4.7 and 4.8 show seven seconds from a typical Working Model 2D rocking simulation. The simulation was started by placing the robot on the ground and allowing the springs to stabilise about their equilibrium point. After this period had elapsed (approx. 0.5 seconds), the robot rocking controller was started. Selected screen shots showing key phases of motion during rocking are shown in figure 4.6.

As can be seen from figure 4.7, after approximately two seconds, steady body pitching with a peak to peak amplitude of 30^o was obtained. Both horizontal and vertical velocities also oscillated repeatable about 0 m/s, resulting in no mean robot displacement. Since the legs had no notion of whether they were in the air or touching the ground, minor tracking errors can be seen γ leg trajectory tracking at leg touchdown impacts.

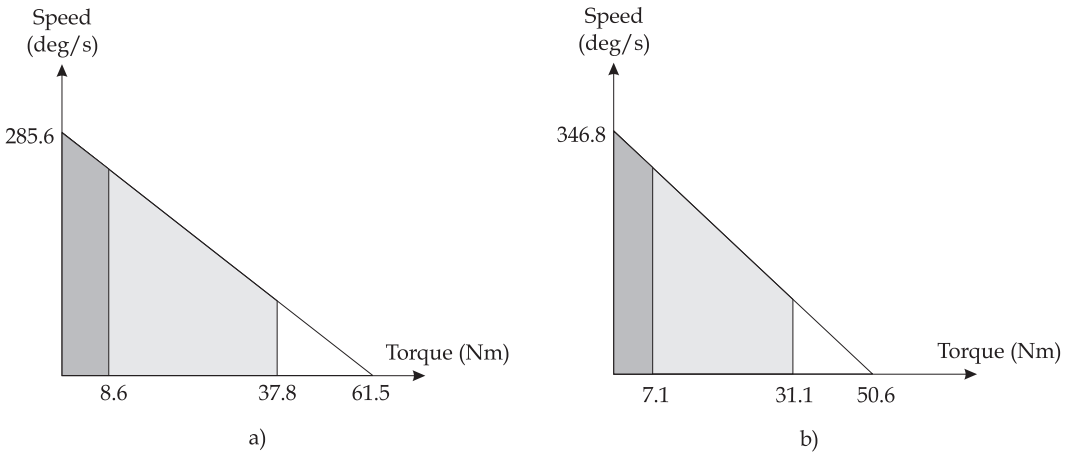

Figure 4.5: First quadrant torque/speed relationship for Scout II's current actuation system. The presented curves assume a) 48/28 sprocket combination b) 48/34 sprocket combination (Assumed efficiencies : $\eta_{gearhead} = 68$ % and $\eta_{belt} = 96$ %). Figure adapted from [6].

Figure 4.9 shows the implemented torque/speed model for all four quadrants of motor operation. Applied torque is also plotted on top of this graph. As can be observed, the output motor torque is clipped to stay within the specified polygon.

4.3.4 Parameter Sensitivity

To study the robustness and sensitivity of the open loop rocking controller, simulations where repeated for variations in controller and robot model parameters.

Since the oscillation amplitude of equation 4.4 is the only user specified controller parameter, this value was first modified. Thus, a set of simulations was performed for which the leg oscillation amplitude was increased in 5^o increments from 5^o to 25^o. Rocking became unstable for oscillation amplitudes exceeding 15^o. This effect is not entirely surprising given that the simple single leg model used to derive the controller did not take into account deviations of the leg from the perpendicular.

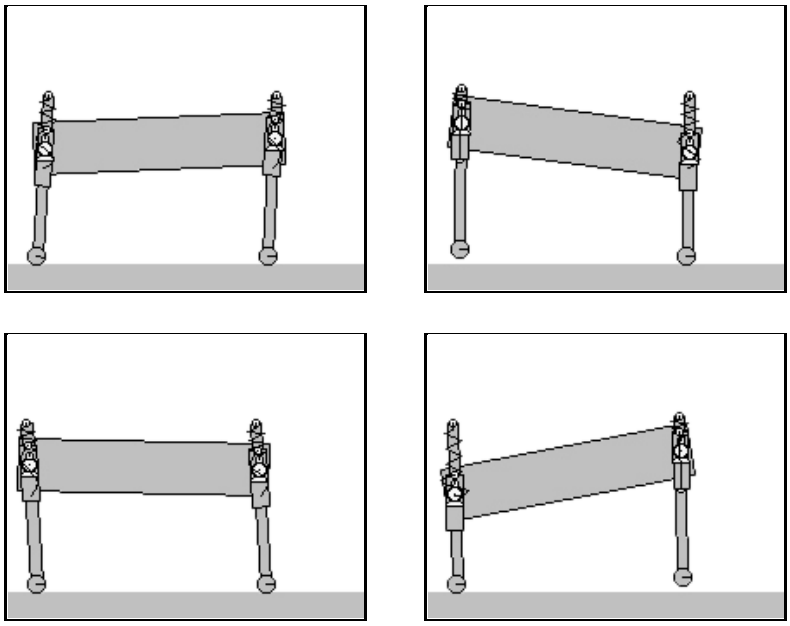

Figure 4.6: Working Model 2D rocking simulation screen shots

Next, physical robot parameters were modified to see what effect modeling inaccuracies would have on eventual rocking on the real robot. To begin, the effect of shifting the body's center of mass (COM) was investigated. To do this, a set of simulations was run for which the COM was shifted in 0.05 m increments towards the front of the robot. The results obtained from these experiments were very promising. Although decreased front foot clearance was observed, simulations showed that for offsets of less than or equal to 0.1 m that the open loop controller still yielded stable rocking. This is quite impressive since a 0.1 m shift in the COM represents about 20 % of the robot's body length. This showed that a large mass imbalance would have to exist in the robot to prevent rocking from working.

Next, linear spring stiffness (i.e. k) was varied $\pm 50\%$ for the front leg. Surprisingly stable rocking was observed for changes in spring stiffness of up to $\pm$ 40%. Changes of spring stiffness greater than 40% resulted in no liftoff of the back leg. Increases of the spring constant also shows large backward motion of the body.

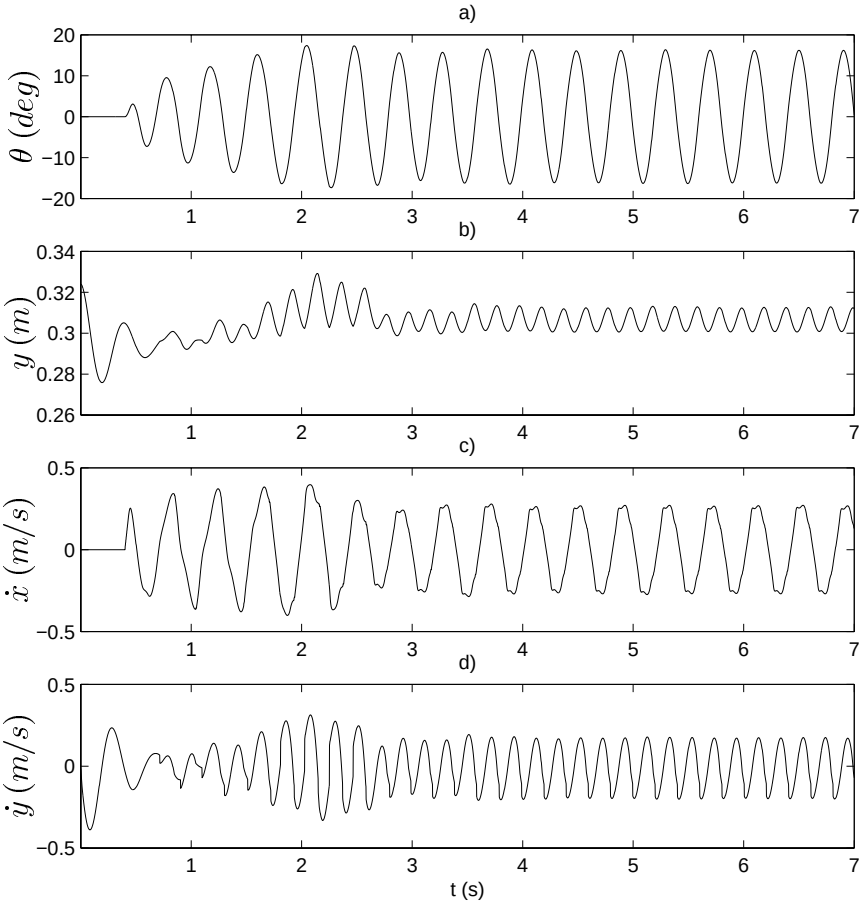

Figure 4.7: Torso behaviour for rocking simulation. a) Body pitch θ (deg.), b) Body height y (m), c) Horizontal velocity $\dot{x}$ (m/s), d) Vertical velocity $\dot{y}$ (m/s).

Once rocking had been investigated, modifications to the rocking algorithm were studied to obtain compliant walking.

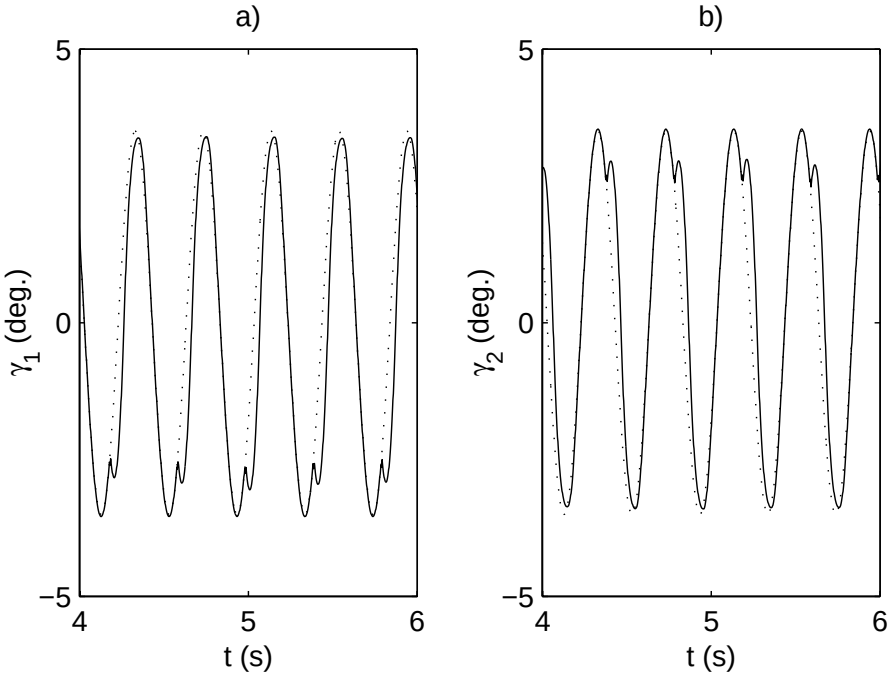

Figure 4.8: Actual (solid) and desired (dotted) leg γ (deg.) trajectories for the a) Front and b) Back legs.

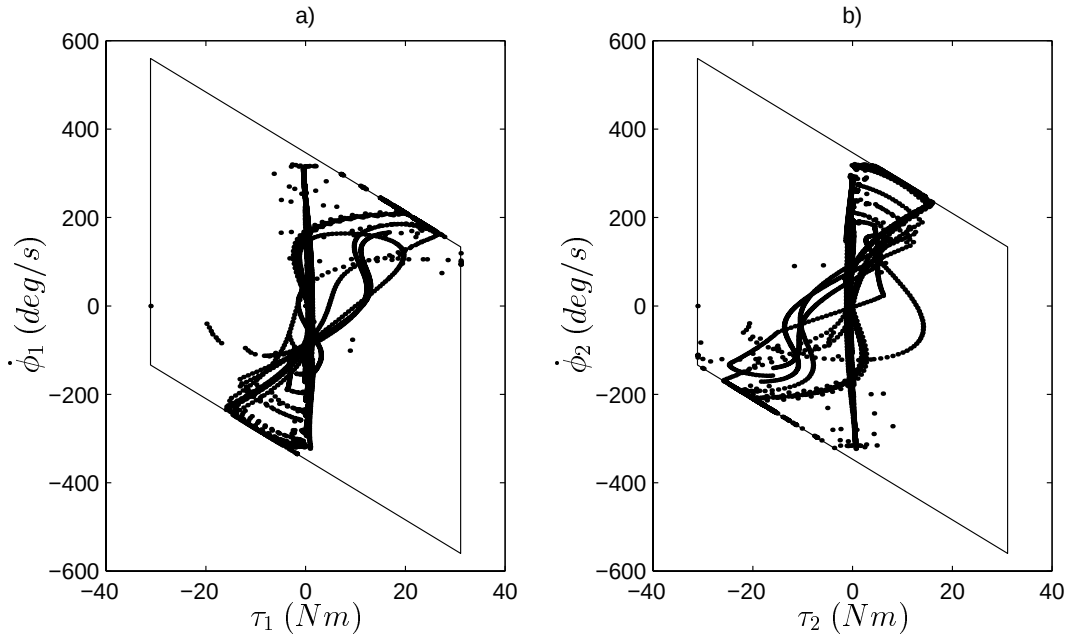

Figure 4.9: Simulation torque/speed motor model. Actual Torque vs. ϕ for the a) Front and b) Back legs.

4.4 Compliant Walking

Robots with articulated legs use the swing phase of leg motion to retract legs, avoid toe stubbing, and position legs for subsequent periods of stance. Since Scout II does not have knees, it relies on steady pitching of the body to maintain alternating periods of leg stance and swing. Therefore, the walk and trot gaits observed in nature are not currently realisable on Scout II. Instead a modified version of the bound, which we call a walking bound, was investigated. This gait differs from the running bound observed in nature since the robot is never ballistic during a locomotion stride.

As can be observed from figure 4.10, during rocking the motion of the back leg synchronised itself independently and with no touchdown feedback to the desired walking behaviour for stance and flight leg phases. The back leg swept backwards, from a positive to a negative angle, during stance and forward during flight. The front leg, however was approximately 180^o out of phase with respect to the desired leg motion for walking. Although this coincided with what would be expected during rocking, the observed leg motion was not suitable for walking.

To solve this problem, a small modification was made to the rocking controller. A two state state-machine was devised, to synchronise leg behaviour, that switched between *stance* and *flight* states for each leg pair. The front and back leg state machines acted independently and without any explicit synchronisation. Figure 4.11 shows the state machine used. Table 4.2 summarises controller actions based the leg state and figure 4.12 shows a controller flowchart.

The walking controller consisted of two main sections: a startup controller and a walking controller. The startup controller used to bring the robot from rest to steady state walking, was the rocking controller described in section 4.3.2. After steady rocking had been reached (a period of approximately 2 sec.), the walking controller was started.

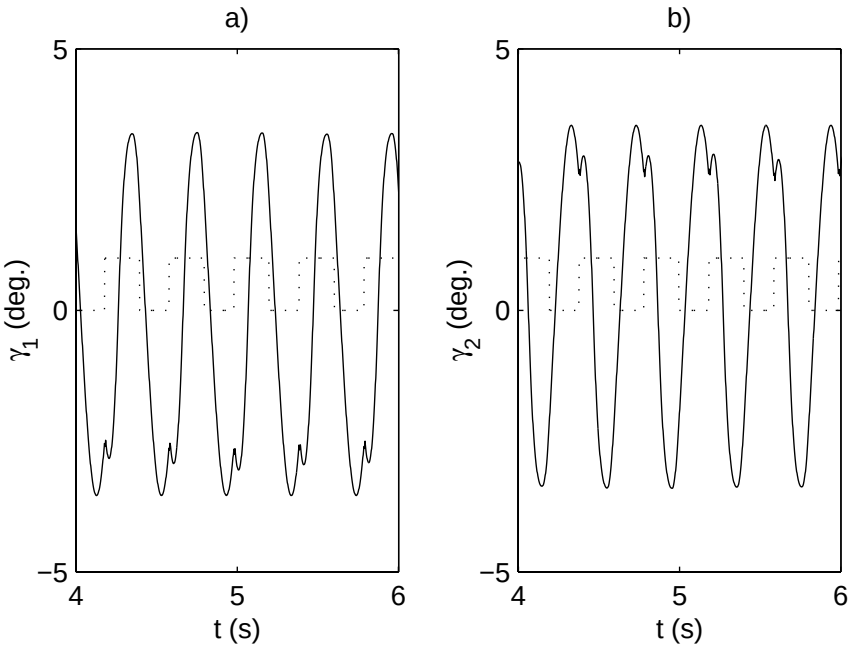

Figure 4.10: a) Front and b) back γ . Leg state are superimposed ($stance = 1$ and $flight = 0$).

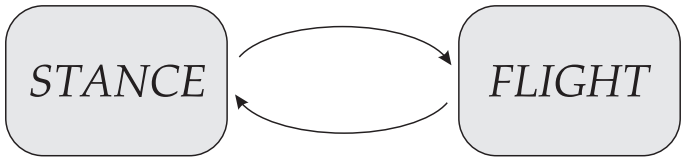

Figure 4.11: Walking leg state machine. Two states are defined : when a leg is in contact with the ground it is said to be in *stance*, otherwise it is in *flight*.

Based on findings from rocking simulations cosinal γ leg trajectories were selected to command to both the front and back sets of legs during stance. During flight, legs were commanded to a set point equal to the amplitude of the stance cosinal trajectory. As in the case of the rocking controller, leg trajectory frequencies were determined by the system natural frequency, using the one leg model of figure 4.3.

Although other leg trajectories could have been chosen, cosinal trajectories offer a few advantages worth noting. Firstly, in the context of the mentioned controller they have first order continuity at the beginning and end

Table 4.2: Compliant walking controller

Legs	State	Action
Front	Stance	$\gamma_f = A_f \, cos \left(\frac{2\pi}{T_{sf}} t \right)$
	Flight	$\gamma_f = A_f$
		$\dot{\gamma}_f = 0$
Back	Stance	$\gamma_b = A_b \, cos \left(\omega_n \, t \right)$
	Flight	$\gamma_b = A_b$
		$\dot{\gamma}_b = 0$

of the trajectory (i.e. 0 velocity), helping to reduce errors in tracking at state transitions. Secondly, commanding zero velocity at the end of leg trajectory has the additional benefit of helping to lower the body onto the front legs at the end of back leg support. This permits the body to oscillate in a natural way. Lastly, the cosinal trajectories are very easy to parametrise in terms of time.

The described controller yielded stable walking, however simulations revealed that the front legs remained in stance for a slightly greater period than the duration corresponding to the natural frequency ω_n. Thus, in order to sweep the front legs with the correct trajectory, the front leg stance duration from the previous stride, T_{sf}, was used as the desired sweep period. Since individual stance and flight periods were recorded during the startup rocking procedure, the equilibrium stance values obtained online were used as an initial stance estimate for the walking controller. To prevent inappropriate stance period values from being used by the walking controller, upper and lower thresholds limits were placed on accepted stance period values. Table 4.3 provides nominal open loop controller values used to obtain steady walking.

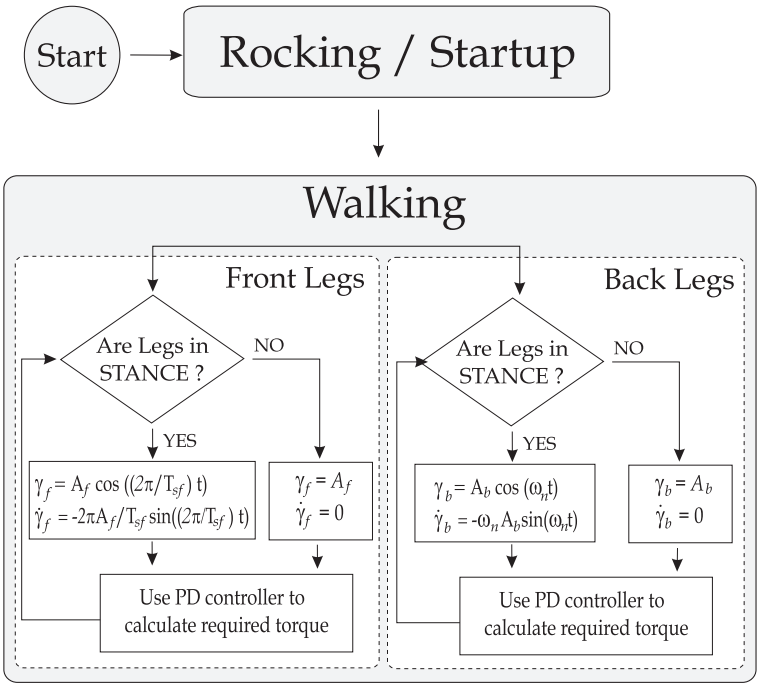

Figure 4.12: Walking controller flow chart

4.4.1 Simulation Results

Figures 4.13 and 4.14, show simulation results from a typical simulation of the walking controller. Figure 4.14 is of particular interest, since it shows that the leg trajectories are properly synchronised with the stance and flight phases. Screen shots from a WM2D compliant walking simulation are also provided in figure 4.15.

Table 4.3: Open loop walking controller values

Parameter	**Value**
ω_n	$15.6\,rad/s$
A_f	7^o [$0.1222\,rad.$]
A_b	10^o [$0.1745\,rad.$]

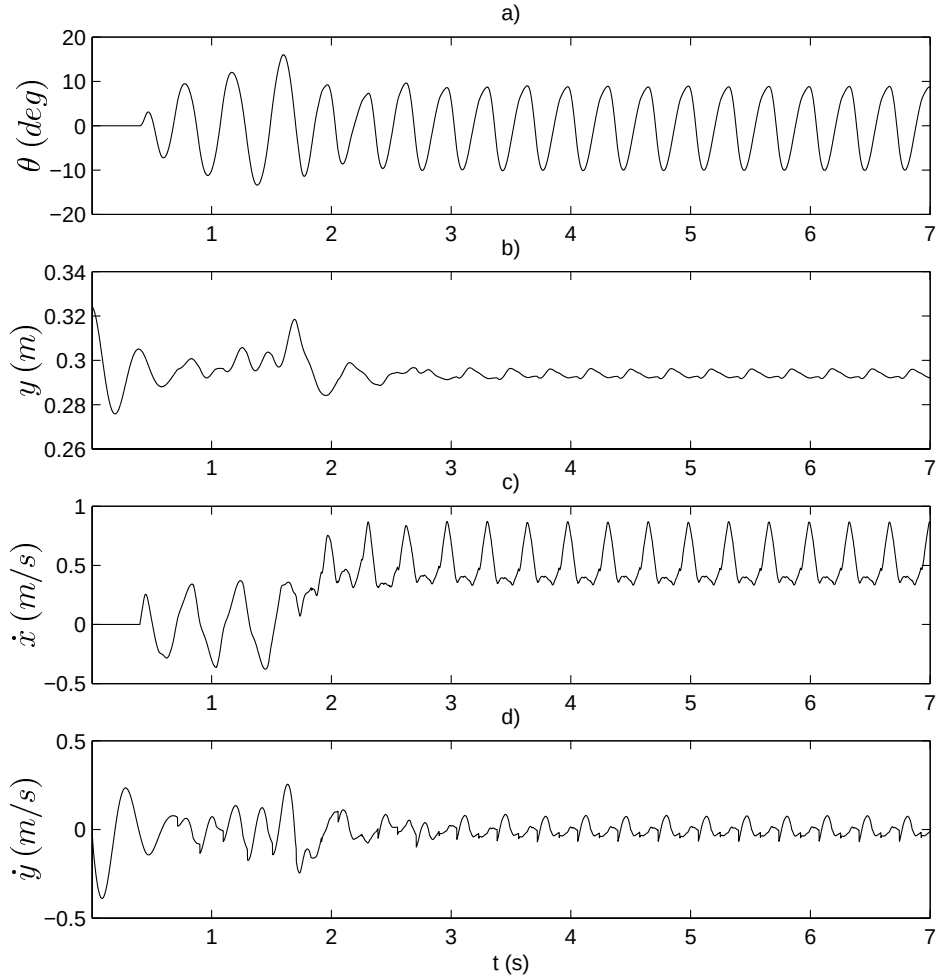

Figure 4.13: Robot torso behaviour during walking.

4.4.2 Parameter Sensitivity

Once the compliant walking controller had been validated in simulation, commanded trajectory amplitudes were varied as a means of obtaining open loop velocity control.

Simulations revealed that the back leg sweep amplitude A_b, had a large impact on the robot's forward velocity. Excessive pitching was observed for back leg amplitudes significantly larger than those of the front leg, A_f. Conversely, if the front leg amplitude, was much larger than the back leg ampli-

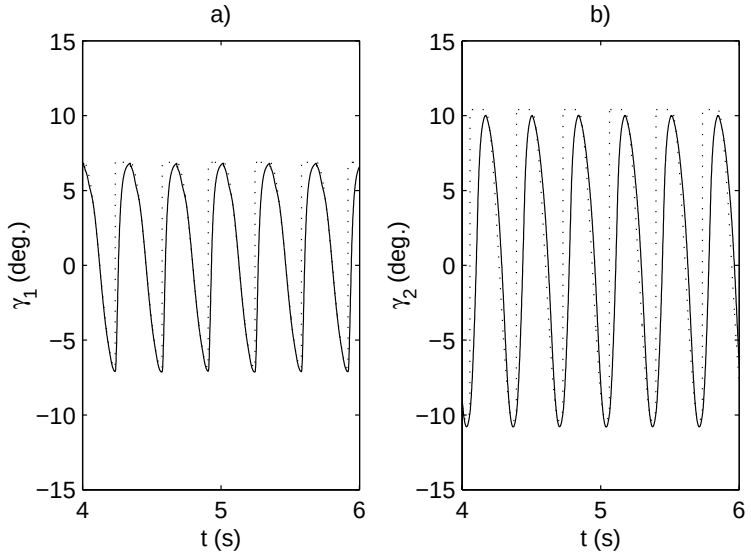

Figure 4.14: Actual (solid) and desired (dotted) walking γ (deg.) leg trajectories for a) front and b) back legs.

tude the likelihood of toe stubbing during brief double stance periods greatly increased. Simulation revealed that maintaining a 3-4^o amplitude difference between front and back legs, resulted in stable compliant walking at a variety of speeds. Using this finding and repeating simulations for various front and back leg amplitudes, the linear map between leg sweep amplitude, and desired forward velocity $\dot{x}_d$ was found to be

$$A_f = 14.866\,\dot{x}_d - 0.55 \quad (4.7)$$

$$A_b = 19.712\,\dot{x}_d + 0.55 \quad (4.8)$$

Figure 4.16 shows the simulation and fit results for the leg amplitude to forward speed function.

To validate this open loop mapping, a simulation was conducted in which the commanded forward speed was ramped up from 0.25 to 0.8 m/s, held at 0.8 m/s, and then ramped back down to 0.25 m/s. Figure 4.17 shows a plot of the actual versus desired velocity obtained from the simulation. Although large deviation exist in the achieved peak forward speed values, a consequence of the robot's leg configuration, good mean velocity tracking was obtained.

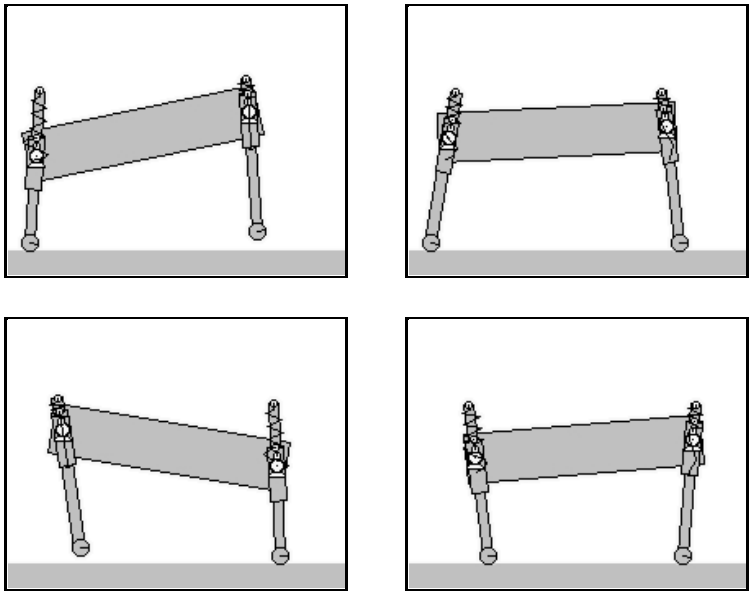

Figure 4.15: Working Model 2D walking simulation screen shots.

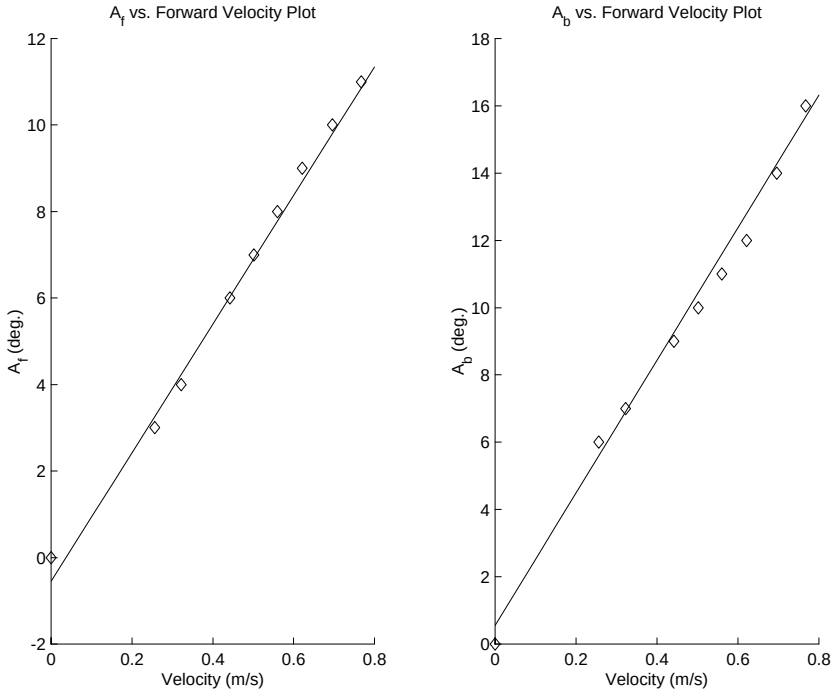

Figure 4.16: Simulation (diamonds) and fit results (solid Line) for A_f and A_b to $\dot{x}_d$ relationship

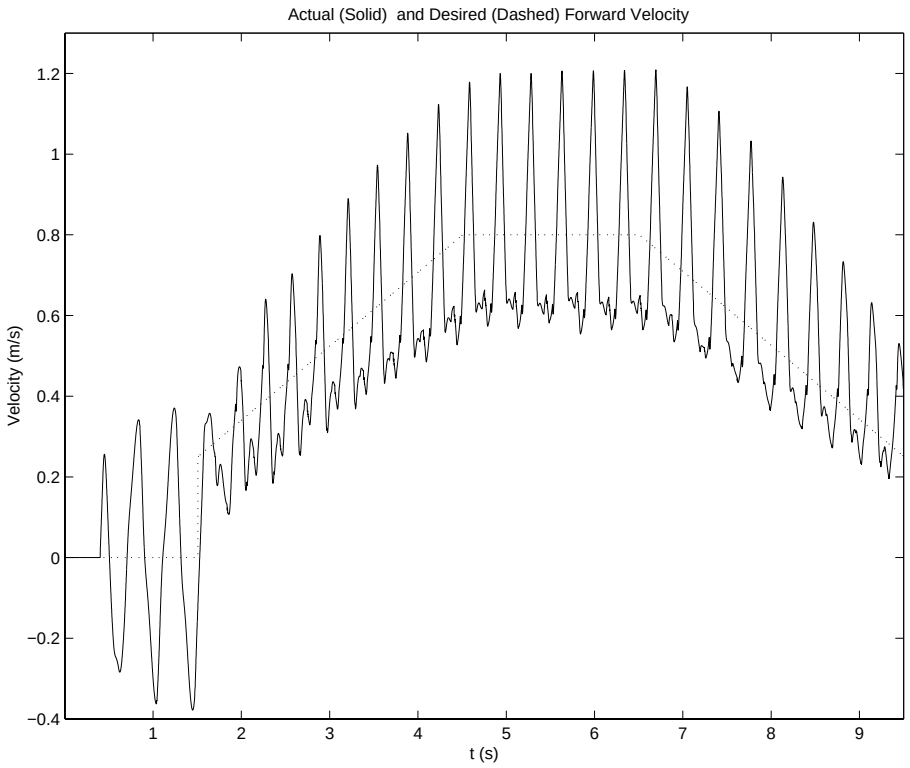

Figure 4.17: Actual and desired forward velocities for walking controller with open loop velocity control

4.5 Summary

This chapter presented modeling considerations used in the study of walking simulations. To conduct these simulations, a physics based two-dimensional simulator was used, allowing simulation of arbitrary rigid bodies systems, without needing to derive the system's equations of motion.

Using a simple planar model for Scout II, it was shown that the model could be further simplified to a single spring/mass/damper system. Using this simple model, the natural undamped and damped frequencies were calculated and the parameter was used to develop an open loop rocking controller. Rocking was studied since it was believe that understanding this behaviour would help to provide a reliable startup sequence for walking. Furthermore, it was anticipated that if a way could be found to excite the system to rock passively, that this would make the development of a walking controller more straightforward.

Using the developed rocking controller, a dynamic compliant walking controller was subsequently derived. Simulations revealed that with only minor parameter modifications that stable walking and open loop velocity tracking could be obtained.

Chapter 5

Experiment

5.1 Overview

Having obtained encouraging Working Model 2D (WM2D) simulation results, the next step was to experimentally verify the developed algorithms on Scout II. Thus the open loop rocking and walking algorithms were both implemented. Unfortunately, these algorithms yielded poor experimental results, with marginal correlation between simulation and experiment. Experimentation revealed some important, yet previously, unmodeled dynamics, helping to explain these differences. Rocking experiments are discusses in section 5.2.

Therefore, another open loop walking algorithm, based on commanding constant horizontal hip velocity for the front and back legs during stance, was experimentally developed. This control algorithm yielded stable dynamic compliant walking and revealed rapid convergence to stable walking. Section 5.3 describes the mentioned walking controller and presents experimentally gathered results. Once a stable open loop walking had been obtained, an energetics analysis was performed to assess the gait's efficiency (see section 5.4).

5.2 Rocking

With simulation results producing stable and robust behaviour for the natural frequency rocking and walking algorithms, the next step was to validate these controllers experimentally on Scout II. Unfortunately, this yielded poor correlation between simulation and experiment. Figures 5.1 - 5.3 shows seven seconds of experimental results from a typical rocking experiment. Although good tracking was observed in both the front and back leg gamma trajectories (see figure 5.2), the front legs remain in contact with the ground, throughout the experiment (see figure 5.3). Of the gathered data, the most significant difference between simulation and experiment was observed in body oscillation amplitude. Recall that rocking simulations yielded peak to peak oscillation amplitude of nearly 30^o (see figure 4.7). Body pitch amplitude during experimental rocking was much less pronounced oscillating between $\pm\ 4^o$.

Repeated experiments showed a random tendency of the system to remain on either front or back legs, with results varying from trial to trial. Although mass imbalance on the robot and variations in leg spring constant were considered as possible causes for this behaviour, tests showed that these sources of error did not exist. Simulations had also indicated that the rocking controller was robust to variations in these parameters (see section 4.4.2).

To further investigate the causes of the large differences observed between experiments and simulation, a series of simple oscillation tests was conducted. This involved placing the robot on the ground, allowing it to reach equilibrium, and giving it a small downward push causing the legs to deflect. Leg deflection profiles were then analysed. These test revealed significantly different profiles than the expected second order spring/damper response, indicating the presence of static friction in the legs. Unfortunately, this factor had not been accounted for in the simulation leg models, explaining the observed discrepancies.

Given these differences and the realization that non-negligeable friction was present in Scout's leg design, we proceeded to develop another controller

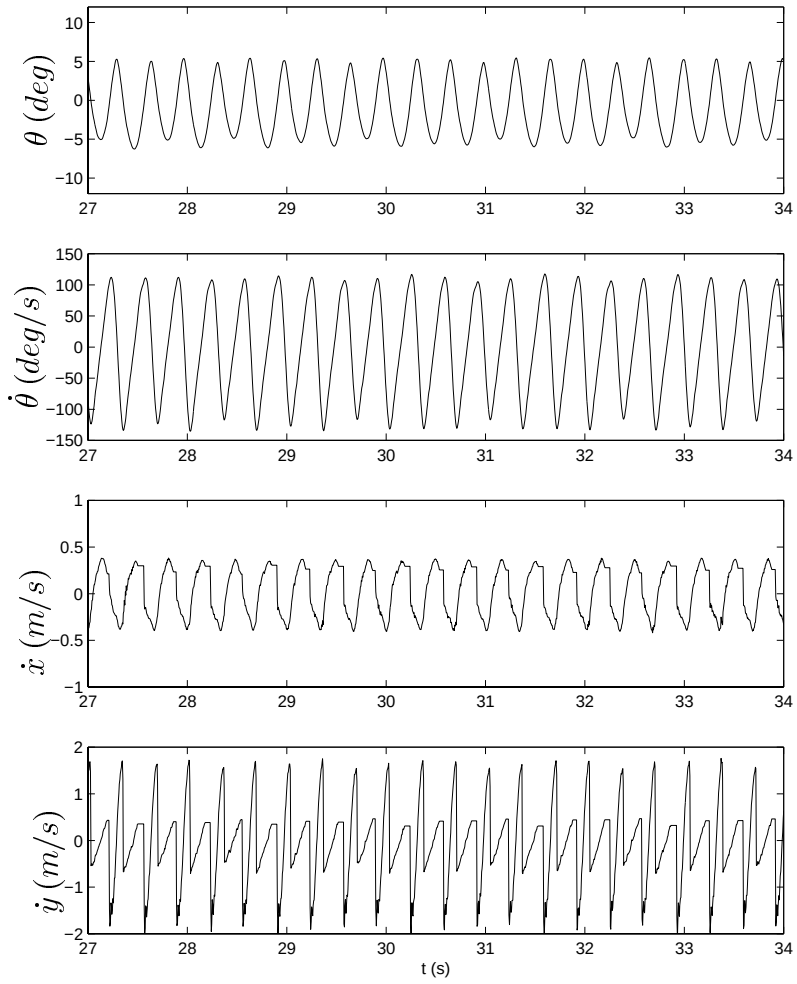

Figure 5.1: Robot torso behaviour during rocking. Presented velocity estimates are calculated online Scout using kinematics.

experimentally.

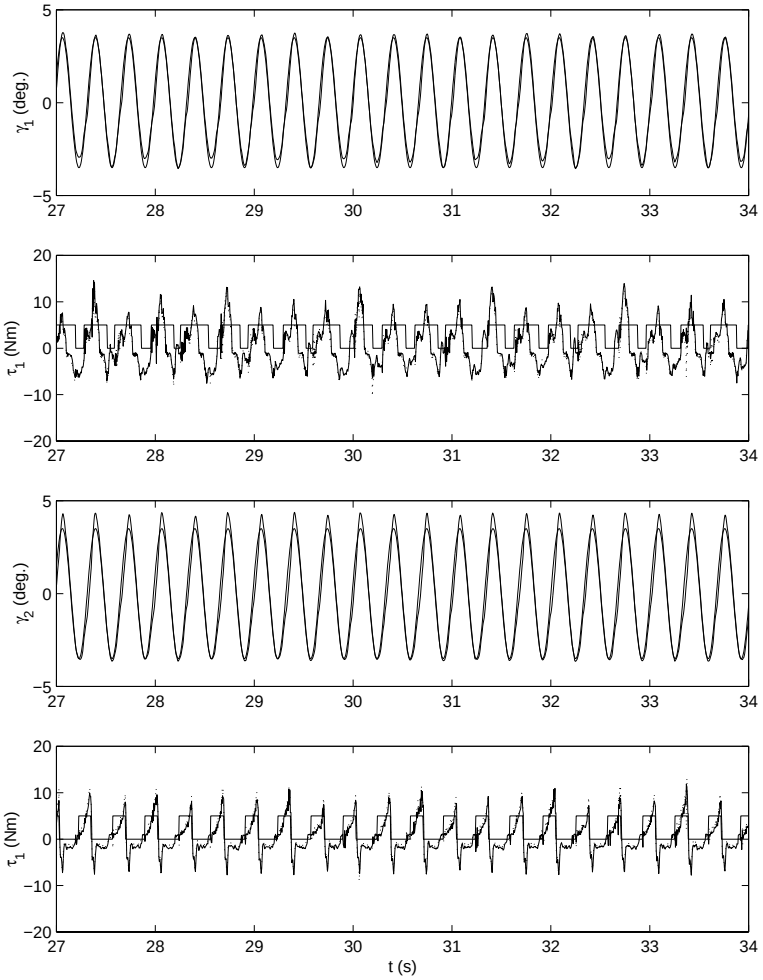

Figure 5.2: Front and back desired (dashed) and actual (solid) leg trajectories and torques for rock with parameters.

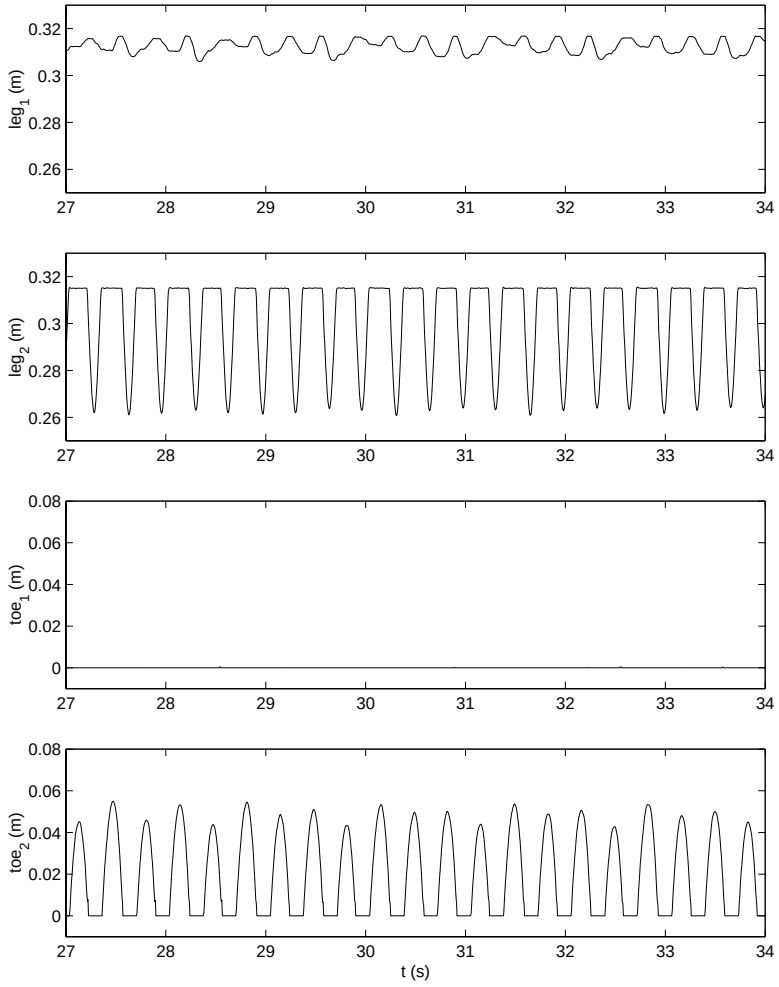

Figure 5.3: Front and back leg lengths and perpendicular ground/toe clearances for rock.

5.3 Walking with Constant Hip Velocity

A key requirement for successful walking is to minimise or eliminate the presence of slipping between support toes and the ground. This is of particular concern in walking, which does not benefit from the same magnitude of normal contact forces, as those typically observed in running. Even the indoor environments of the research lab can pose significant challenges to a walking robot if slip cannot be detected and avoided. In steady state stable walking if the robot hips travel at the same speed as the center of mass of the body (COM), the toe will not experience slip, with this approach being principally constrained by the grounds Coulomb friction factor. With this in mind, a simple dynamic walking control strategy was devised.

Preliminary experiments revealed that front and back legs play markedly different roles in quadrupedal walking. In contrast to the back legs that provide bulk forward propulsion for locomotion, the front legs act as brakes slowing the forward motion of the body, helping to lift the back legs off the ground. Given this antagonist relationship, a controller using slightly different control strategies for front and back pairs of legs was developed. Figure 5.4 shows a planar model of Scout II used to develop the constant hip velocity controller described below. Adopted nomenclature is also shown.

As with the dynamic walking controller developed in simulation, a two state leg state machine was used to synchronise leg actions (see section 4.4). To ensure that controller actions were synchronised for front and back lateral leg pairs, the state machine changed state based on the state of a virtual leg formed by grouping left and right legs at each hip. This approach was motivated by the previous work of Sutherland [59], Raibert [54], and Papadopoulos [49]. Although similar in flavour, it should be noted that in the context of this controller the virtual leg idea was used as a synchronisation mechanism rather than as a means of equalising support force. This mechanism ensured that before triggering a state change for front or back legs, that lateral leg pair states were consistent.

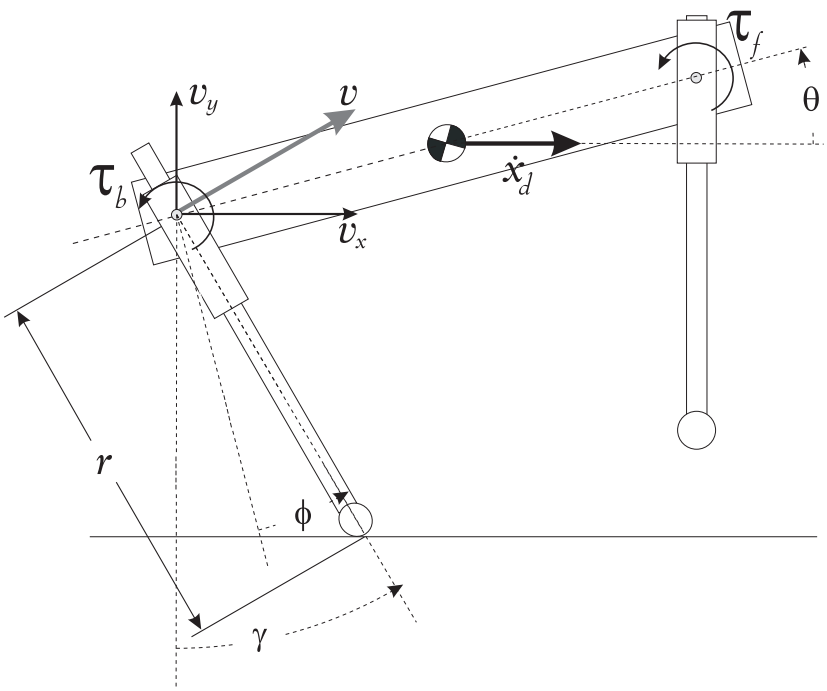

Figure 5.4: Planar Scout II controller model showing key nomenclature.

As shown in table 5.1, a similar strategy was used for both the front and back legs during stance and flight. During flight, both front and back pairs of legs were servoed to a desired touchdown angle, γ_{dtdf} and γ_{dtdb}. In stance, the back legs were commanded to sweep backwards, tracking a user specified horizontal hip velocity, $\dot{x}_d$, matching the *desired* horizontal velocity of the robot's COM. A similar approach was used for the front legs, who were commanded to track a fraction of the desired back leg speed determined by $\dot{x}_{ratio}$. Since both the leg length and the γ leg angle varied for each leg during periods of leg stance, the desired position trajectory was obtained by integrating the desired angular velocity, $\dot{\gamma}_d$, trajectory using a trapezoidal integrator.

As with previous controllers, a *proportional derivative* (PD) servo,

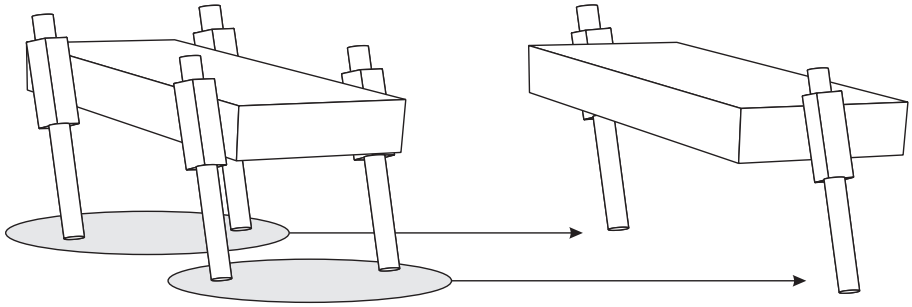

Figure 5.5: Virtual Leg Model. By pairing left and right legs at each hip it is possible to base controller actions on the behaviour of the resulting imaginary leg.

$$\tau_i = \kappa_p \left(\gamma_i - \gamma_{d\,i}\right) + \kappa_v \left(\dot{\gamma}_i - \dot{\gamma}_{d\,i}\right) \tag{5.1}$$

was used to calculate torque to command to the motors. Experimentally used PD controller gains are listed in table 5.2.

Once implemented, a heuristical search of the controller's parameter space was performed to find controller values yielding stable open loop walking behaviour. Table 5.3 presents these values. A formal discussion of experimental results is presented in section 5.3.1. Controller sensitivity and robustness are discussed in section 5.3.3.

5.3.1 Experimental Results

To validate the proposed walking algorithm, a set of experiments was conducted on Scout II. These experiments yielded stable walking, despite a simple open loop control strategy using two decoupled state machines. Figure 5.6 shows snapshots from a typical locomotion stride from one of these experiments. The presented frames show key phases of motion during walking, including back (1) and front support (3), as well as intermediate periods of double support (2,4). Ten seconds of experimental results for another experiment are shown in figures 5.7 - 5.9.

Table 5.1: Open loop constant hip velocity controller.

Legs	State	Action
Front	Stance	$\gamma_{d\,i} = \int \dot{\gamma}_{d\,i}\, dt$
		$\dot{\gamma}_{d\,i} = \frac{\dot{x}_d}{r_i(t)\, cos(\gamma_i(t))}\, \dot{x}_{ratio}$
	Flight	$\gamma_{d\,i} = \gamma_{d\,td\,f}$
		$\dot{\gamma}_{d\,i} = 0$
Back	Stance	$\gamma_{d\,i} = \int \dot{\gamma}_{d\,i}\, dt$
		$\dot{\gamma}_{d\,i} = \frac{\dot{x}_d}{r_i(t)\, cos(\gamma_i(t))}$
	Flight	$\gamma_{d\,i} = \gamma_{d\,td\,b}$
		$\dot{\gamma}_{d\,i} = 0$

Table 5.2: Experimental PD controller gains.

State	Gain
Stance	$\kappa_p = 9.599\ Nm/deg$ [$550\, Nm/rad$]
	$\kappa_v = 0.436\ Nms/deg$ [$25\, Nms/rad$]
Flight	$\kappa_p = 6.109\ Nm/deg$ [$350\, Nm/rad$]
	$\kappa_v = 0.175\ Nms/deg$ [$10\, Nms/rad$]

As can be observed from figure 5.7, the body pitches repeatably with a peak to peak amplitude of approximately 15^o at a frequency of $1.5\, Hz$. The body pitching rate, $\dot{\theta}$, was also very repeatable. Observed mean perpendicular ground/toe clearances for the front and back toes were of 0.015 and 0.06 m respectively (see figure 5.9).

Figure 5.8 clearly shows the previously mentioned antagonistic behaviour of the front and back legs. The front legs can be observed as applying mostly positive torque during stance, acting to brake the body. This occurs because when the front legs hit the ground, impacts tend to push them in the negative

Table 5.3: Open loop constant hip velocity controller parameters.

Parameter	Value
γ_{dtdf}	0^o [$0\,rad.$]
γ_{dtdb}	26^o [$0.453\,rad.$]
$\dot{x}_d$	$0.2\,m/s$
$\dot{x}_{ratio}$	15 %

direction, thus increasing position tracking errors. To compensate for this error, a positive hip torque is applied by the robot, resulting in a clockwise couple on the body, helping to lift the back legs off the ground. Conversely, the back legs apply a negative torque during stance helping to propel the body forward. Considerable tracking error also develops in the back legs in part due to the large impacts during state transitions from flight to stance (see figure 5.8). A formal discussion tracking error sources is presented in section 5.3.2.

In terms of forward velocity tracking, although we are commanding the back legs to track $\dot{x}_d = 0.2\,m/s$, the mean forward velocity of the COM closer to $0.128\,m/s$ [1], revealing a mean velocity tracking error of approximately 35%. A close look at the forward velocity profile of the body reveals peak velocity values alternating between 0.5 and $-0.2\,m/s$. This large deviation is consistent with forward speed variations for the compliant walking algorithm described in section 4.4.

A close look at the commanded and actual front leg trajectories (see figure 5.8), helps to explain some of these variations. Although the front legs are commanded to sweep in stance, they only move about 2.5^o, with half of the deflection resulting from poor tracking. These errors are a consequence of the significant impacts experienced by the front legs at touchdown and from belt backlash in Scout's actuation system. Given this minor front leg displacement, the front legs can be thought of as remaining fixed throughout

[1] calculated off line from data shown in figure 5.7.

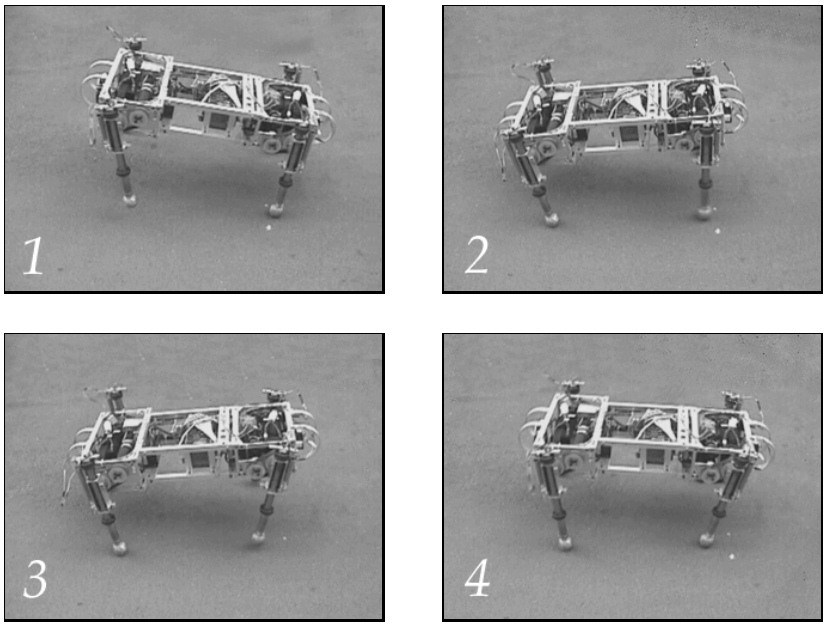

Figure 5.6: Key frames of Scout II in a bounding walk. Four distinct phases are observable : 1) Single Support (Back), 2) Double Support (Back to Front), 3) Single Support (Front), and 4) Double Support (Front to Back)

the stride. This is consistent with previous findings by Yamazaki [64] who obtained stable open loop stiff legged walking, by commanding the front leg to remain perpendicular to the body (refer to section 2.4.3 for more details). The sharp decelerations in forward velocity resulting from maintaining the front legs fixed, contribute to lifting the robot's hind legs off the ground, at the expense of producing large variations in forward speed.

Figure 5.9 also provides insight into some important, yet previously unmodeled system dynamics. As can be seen from this figure the back leg deflection does not match the parabolic profile expected for a spring mass system sliding in a frictionless slot. The plotted data clearly shows that the back leg length actually remains constant for significant portions of the stance period. This further emphasises the presence of significant Coulomb friction in Scout II's current leg design (as mentioned in section 5.2).

Since Coulomb friction is proportional to the normal leg contact force, it makes sense that its effects would be more pronounced on the back rather

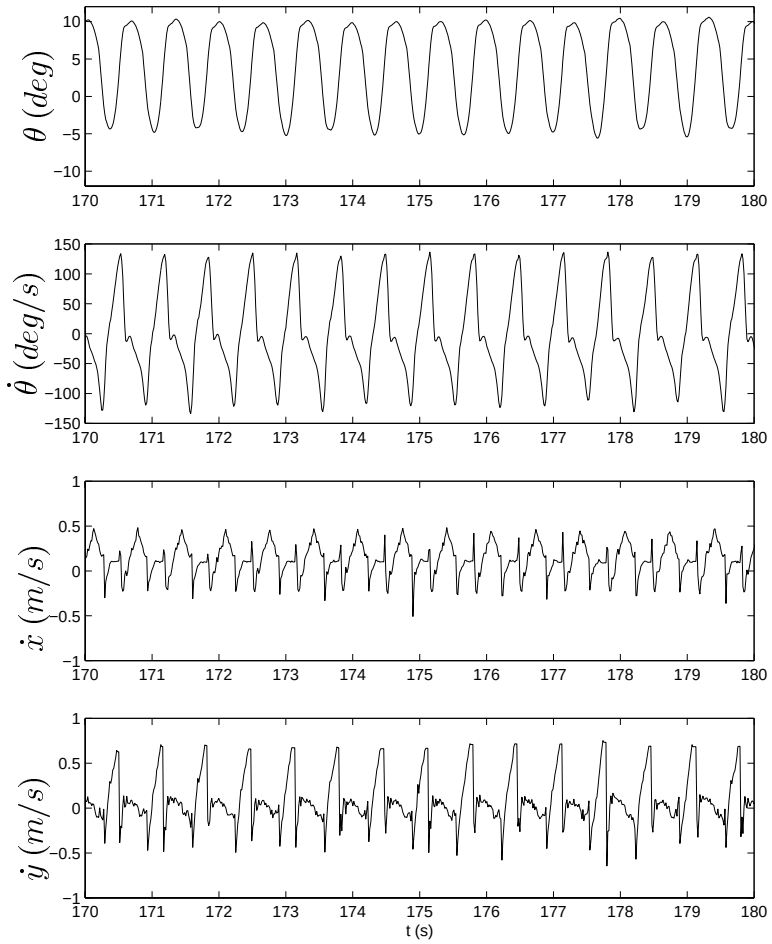

Figure 5.7: Robot torso behaviour during constant hip velocity walk with parameters from table 5.3. Presented velocity estimates are calculated online Scout using kinematics.

than the front legs. Not only do the back legs apply larger torques for more significant periods of time (i.e. the back stance period is much larger than that of the front leg) than the front legs, but the back legs must also actively support all of the robot's weight, while trying to propel the robot forward.

Despite these controller characteristics, the proposed dynamic compliant walking algorithm proved quite stable converging quickly to steady state walking. Variations in terrain slope and ground friction, had minor yet observable effects on controller performance.

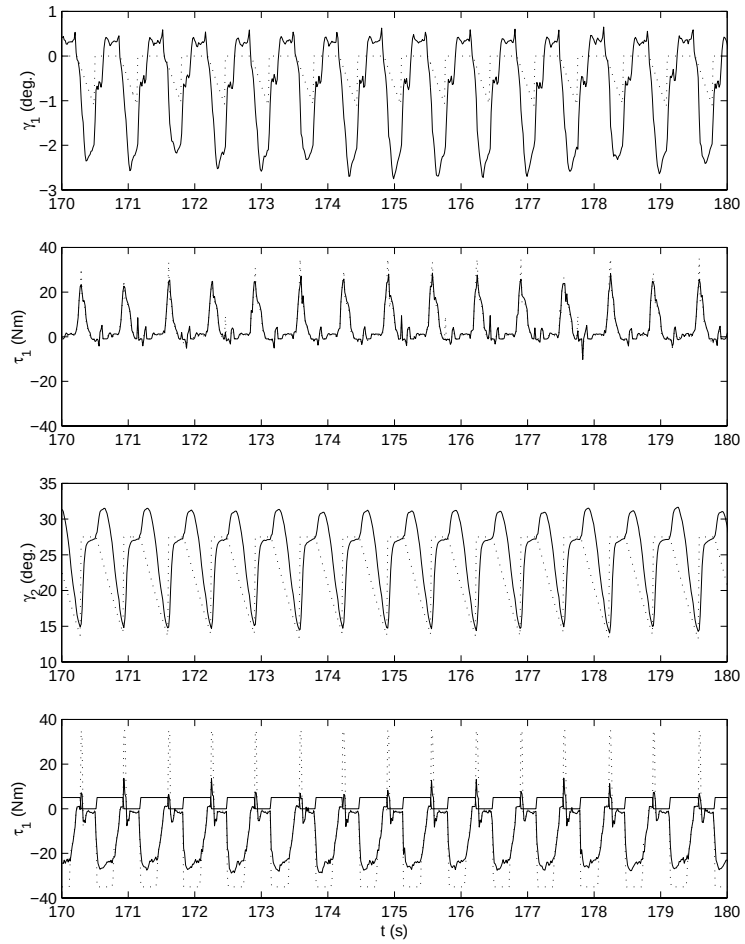

Figure 5.8: Front and back desired (dashed) and actual (solid) leg trajectories and torques for walk with parameters from table 5.3.

5.3.2 Actuator Limits

Although stable and repeatable walking was obtained for Scout, one issue which remains to be addressed in our discussion of experimental results, is the discrepancy between commanded and applied motor torques observed in figure 5.8. Similar errors can also be seen in the front legs, however they are much less severe. Understanding the source of these errors can potentially help improve trajectory tracking in our walking algorithm or influence the design of future walking algorithms.

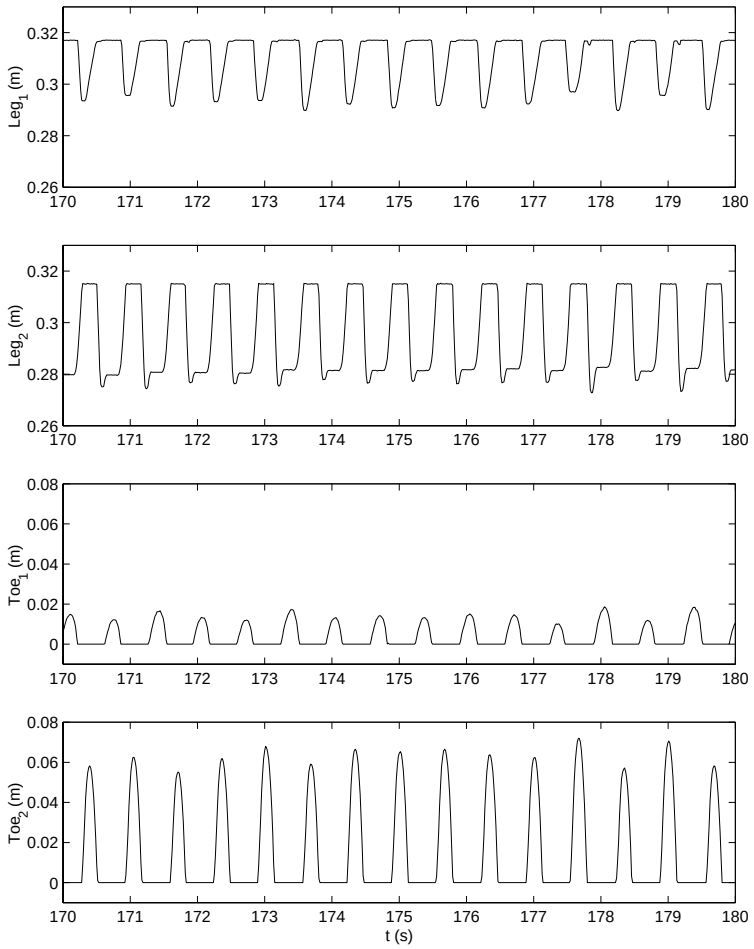

Figure 5.9: Front and back leg lengths and perpendicular ground/toe clearances for walk with parameters from table 5.3.

Given Scout's requirements for autonomous operation, we must use light weight motors to extend operating life. Unfortunately, as touched upon in sections 1.3 and 4.3.2, this has the undesirable side effect of forcing actuators to be used in peak power regions, where the maximum achievable torque is highly dependent on motor velocity.

Currently, Scout uses four *Maxon 118777 brushed 90 W DC motors*, each controlled by a *Advanced Motion Controls 12A8E* PWM servo amplifier [16]. These motors operate at 24 V, a limit set by the robot's batteries, and are current limited to 12 A, a constraint imposed by the motor amplifiers.

Given these operating conditions, the torque/speed characteristics previously shown in figure 4.5 determine the allowable motor torque that may be delivered by the motor at a particular shaft speed. Figure 5.10 shows the applied torques versus angular speed for legs one and two during] a typical walking experiment. As can be observed, the applied torques remain inside the torque/speed polygon specified by the motor model. It is interesting to note, however, that there is still a discrepancy between the theoretical torque limit and the torque applied in experiment (as shown in figure 5.10), since applied torque does not reach the polygonal torque limits.

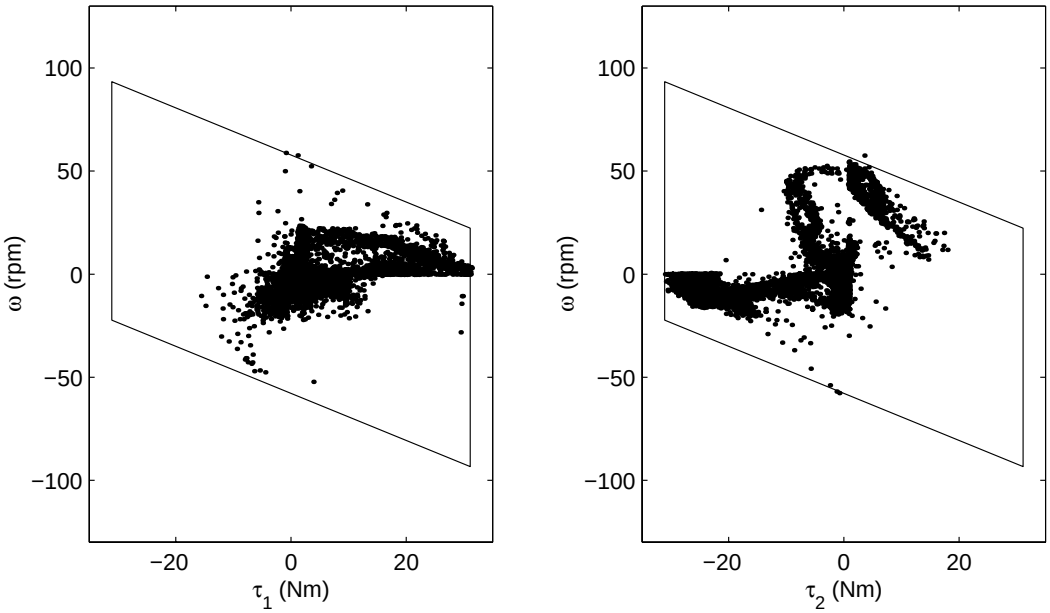

Figure 5.10: Applied front and back leg torque vs. speed : Experiment. The motor's torque/speed limits restrict applied torques at a particular velocity to remain inside the indicated parallelogram.

Using the simple DC motor model of figure 5.11, and applying Kirchoff's voltage law, the motor terminal voltage V_T can be shown to be,

$$V_T = i_A R_A + E_A + L_A \frac{di_A}{dt} \tag{5.2}$$

where R_A is the armature resistance, E_A is the motor back EMF, L_A

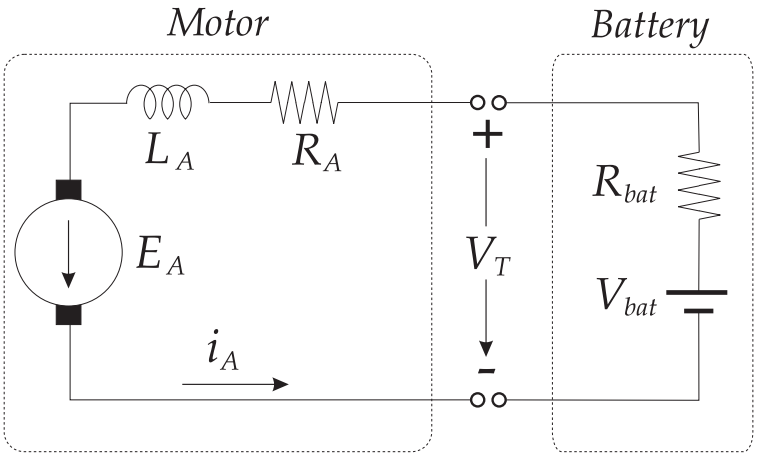

Figure 5.11: DC Motor and Battery Model

is the motor inductance, and i_A is the motor current. Assuming quasi-static motor operation (i.e. $\frac{di_A}{dt} \approx 0$) and using the fact that,

$$E_A = K_\omega \, \omega \tag{5.3}$$

$$\tau = K_T \, i_A \tag{5.4}$$

it can be shown that the maximum achievable motor torque τ that can be produced at a particular velocity ω is,

$$\tau = \frac{K_T}{R_A} \left(V_T - K_\omega \, \omega \right). \tag{5.5}$$

In equation 5.5, K_T is the motor torque constant and K_ω is the motor speed constant. Key motor parameters are summarised in table 5.4.

Furthermore, using a simple battery model, the terminal voltage V_T can be further expressed as,

Table 5.4: Parameters used for voltage compensated torque/speed limit.

Parameter	Value
K_T	$0.0389\ Nm/A$
K_ω	$0.00406\ V/rpm$
R_A	$1.23\ \Omega$
$N_{gearhead}$	$72.38 : 1$
η_{belt}	0.8

$$\begin{aligned} V_T &= V_{bat} - R_{bat}\, i_A \\ &= V_{bat} - \frac{R_{bat}\, \tau}{K_T} \end{aligned} \tag{5.6}$$

thus reducing equation 5.5 to,

$$\tau = \frac{K_T}{R_A \alpha}\ (V_{bat} - K_\omega\, \omega) \tag{5.7}$$

where $\alpha = \left(1 + \frac{R_{bat}}{R_A}\right)$.

Figure 5.12 helps better understand the significance of equation 5.7. Specifically, figure 5.12b shows the large differences that exist between commanded (dash-dot line) and applied motor torques (solid line) during a typical period of back leg stance.

Recall that so far our discussion of the motor torque/speed limit has assumed 24 V operation. Plotting equation 5.5 with $V_T = 24$V on figure 5.12b (dotted line) shows that the nominal motor voltage accounts for a large portion of the errors. As shown in figure 5.12a, however, the motor terminal voltage drops far below 24 V during normal operation (a result of the battery's internal resistance). Recalculating, the maximum achievable torque as per equation

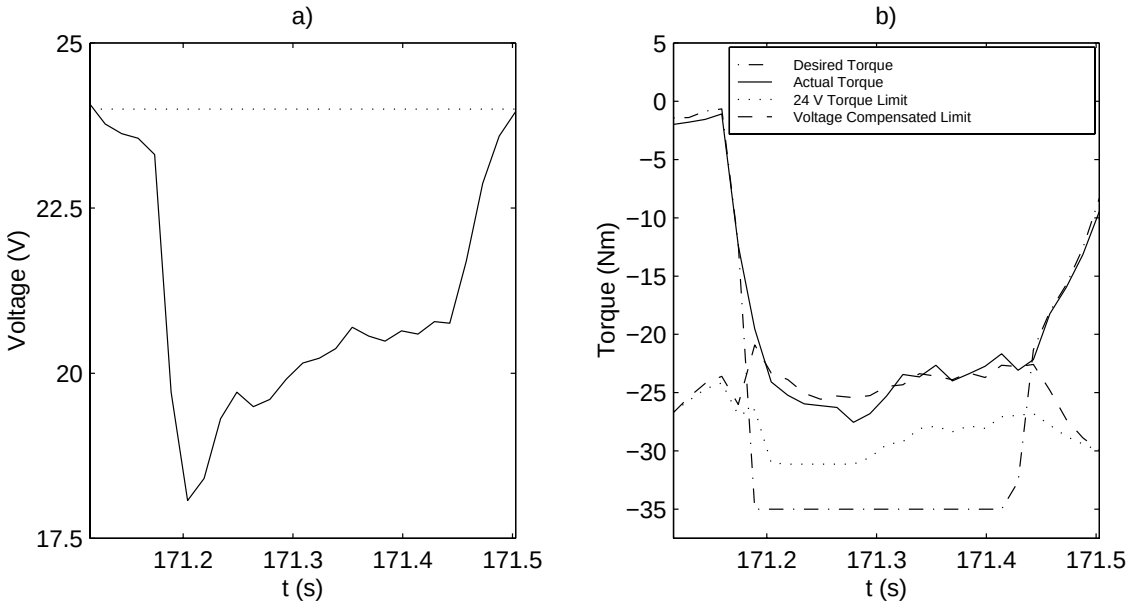

Figure 5.12: a) Supply voltage during a walking stride. b) Actual (solid), desired (dash-dot), 24 V limit, and voltage compensated torques for a walking stride : Experiment

5.7 given the terminal voltage, accounts for remaining errors in torque and provide an excellent match to experimentally applied torque (dashed line).

Figure 5.13, shows that using the measured battery current and an internal battery resistance $R_{bat} = 0.25\,\Omega$, we can get a good match between measured motor terminal voltage (solid line) and estimated terminal voltage (dotted line).

5.3.3 Open Loop Controller Stability

To test controller stability an experiment was conducted in which the robot walking procedure was started under three different conditions. Firstly, a robot walk was started using a normal startup procedure. This was done by leaning the robot onto its front legs and giving the body a small negative pitch. Secondly, the robot was started from a large negative angle of approximately -30^o. Lastly, the walk was started by placing the robot on its back legs

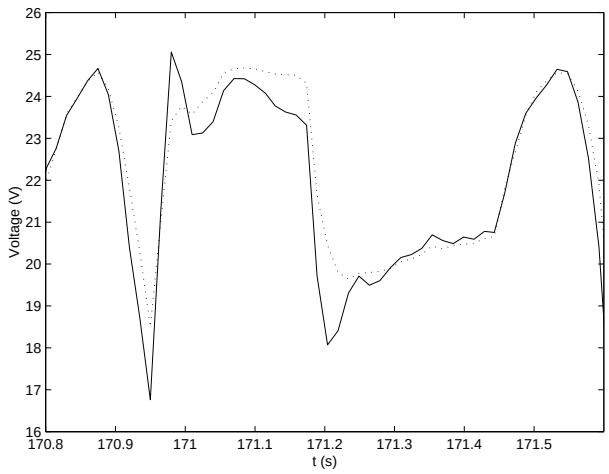

Figure 5.13: Motor terminal voltage (solid) and calculated battery voltage based on internal battery resistance (dotted line) using internal battery voltage $V_{bat} = 25V$, $R_{bat} = 0.25\Omega$, and current drawn during operation i_A: Experiment

and giving the body a large positive angle of approximately 30^o. As can be observed from figure 5.14, for all three vastly different startup conditions, the maximum body pitch of the robot, θ_{max}, converged back to the nominal pitch walking value within three strides. Stable walking was observed in all three cases.

These results are encouraging and validate the stability of the open loop walking controller. However they are also not entirely surprising given our previous observations of lossy dynamics mentioned in section 5.3.1. Since the passive unforced system response is almost completely attenuated by the high system losses, convergence is almost entirely dependent on the energy added to the system by the controller. Therefore, although the controller was stable, this came at the expense of a walking gait requiring substantial power.

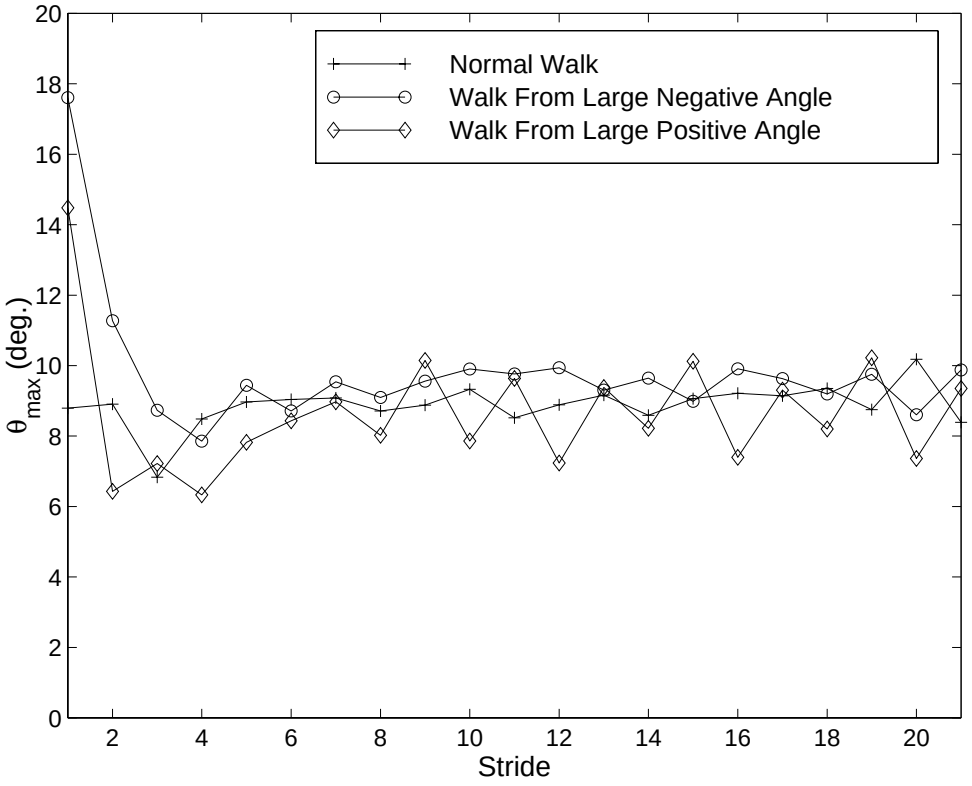

Figure 5.14: Open loop controller stability test results. The walking controller is started from three different conditions : 1) Normal startup condition 2) Startup from large negative angle 3) Startup from large positive angle.

5.4 Walking Energetics

One of the strong motivations for the study of underactuated legged robots is that reducing actuated degrees of freedom and exploiting passive dynamical system behaviour can lead to substantial energy savings. However, to be able to objectively compare energy consumption of various systems (both legged and wheeled) a fair measure must be used that takes vehicle weight, size, speed, and configuration into account. In 1950, Gabrielli and von Kármán [22] proposed a measure of locomotion energetics called *specific resistance* (ε),

$$\varepsilon = \frac{P}{m\, g\, v_{max}}. \tag{5.8}$$

Specific resistance is defined as the ratio of output power P, to the product of maximum speed v_{max}, and vehicle weight $m\,g$. This expression can be further generalised to,

$$\varepsilon(v) \;=\; \frac{P\,(v)}{m\,g\,v} \tag{5.9}$$

to measure ε at various locomotion speeds. By plotting ε against speed, Gabrielli and von Kármán compared the energetic performance of land, air, and sea vehicles, as well as of biological systems of the same scale.

More recently Gregorio and Buehler [28] presented a comparative study of the specific resistance of animals, as well as wheeled and legged vehicles/robots. Their study, found large variations in the literature with respect to how output power was measured for each vehicle. Cars tended to quote power at maximum acceleration, rather than maximum speed. Other vehicles, which reported low specific resistances, made use of short term power storage devices, such as flywheels, reducing power consumption. Published results also neglected to take into account that in contrast to many conventional wheeled vehicles, which carry their power sources, few legged robots currently do so.

In addition to the above inconsistencies, the issue of which type of power to consider is also not clear. To date, most robotics researchers have used use mechanical power when evaluating system power consumption [28, 51]. Although this provides useful insight into system energetics, yielding a platform independent measure of efficiency it does not tell the whole story. Given the increasing amount of electronic hardware on robots and the fact that mechanical power does not account for the significant energy losses due to heat dissipation, which can be quite significant for conventional electric actuators, a more realistic measure of system energetics should be based on electrical power.

Thanks to some custom hardware recently integrated onto Scout II, we have been able to measure electrical voltage and current levels throughout

experiments. In the near future, this capability will allow online battery capacity estimation letting Scout know how much useful operating life remains before it needs to "ask" for a recharge. This may also allow the robot to automatically transition between different gaits in order to operate optimally at various travel speeds. Figure 5.15 shows the obtained measurements for battery voltage and current for the same ten second walk shown in figures 5.7 - 5.9. As touched upon in section 5.3.2, both battery voltage and current deviate significantly from steady state values during normal operation of the robot. Voltage can be seen to reach peak values between 17 - 24.5 V. Current also oscillates repeatedly between 2 - 25 A. Figure 5.16 shows the calculated electrical and mechanical power from the robot. Electrical and mechanical power are calculated via,

$$P_{electrical} = V\,I \tag{5.10}$$

$$P_{mechanical} = \sum_{i=1}^{4} \mid \tau_i\,\dot{\phi}_i \mid \tag{5.11}$$

respectively. As anticipated the difference between input electrical power and output mechanical power is significant. For a mean input power of 234 W output mechanical power is 24 W, about one tenth the input power.

To obtain an estimate of specific resistance for Scout II, data from 10 walking experiments was gathered. Given the narrow range of operation speeds for the open loop controller, specific resistance could only be found for velocities ranging from $0.09 - 0.15\ m/s$. Average velocity, as well as electrical and mechanical power consumption for each of these experiments was calculated. Once plotted a second order least square regression was fit to the obtained data.

The results from this analysis are very encouraging. Plotted estimates of ε using mechanical power in figure 5.17 yield specific resistance values as low as those for Monopod II (0.7) [1, 2], one of the most efficient robots to

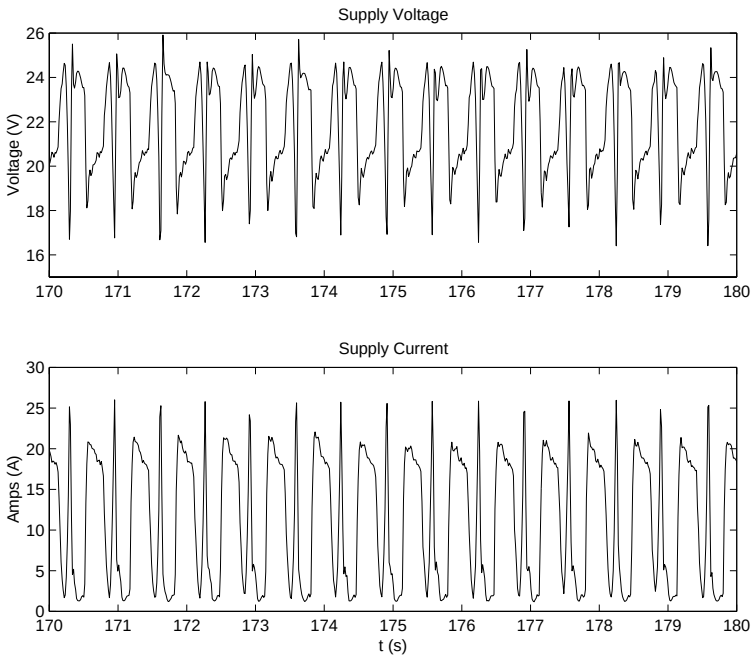

Figure 5.15: Battery voltage and current measurements obtained from the robot for a typical 10 second walk. Controller settings for this walk are listed in table 5.3.

date, even though we know from previous discussion that few passive dynamical effects are currently being used by Scout in walking. Although it still remains to be experimentally confirmed, it is believe that even lower specific resistance values could be obtained for running gaits, since the robot will be travelling substantially faster, with similar power requirements. A perhaps less encouraging realisation is the need to improve Scout's electrical efficiency, since the low 10% efficiency leaves much to desire. This issue will need to be addressed if the robot is ever to be used in real life applications, that require substantial periods of operation between recharges.

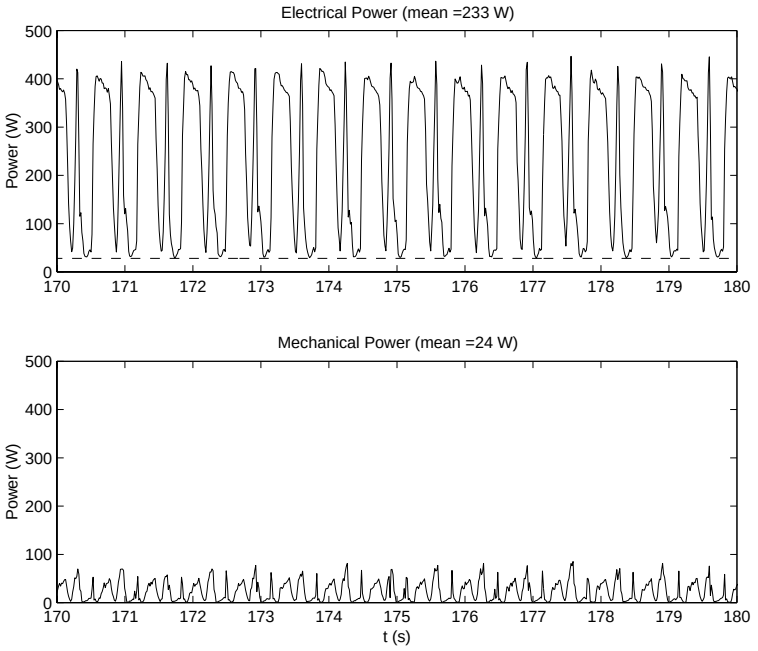

Figure 5.16: Electrical and mechanical power for 10 second open loop walk whos controller settings are listed in table 5.3. 28 W steady state electrical power indicated by dashed line in top plot.

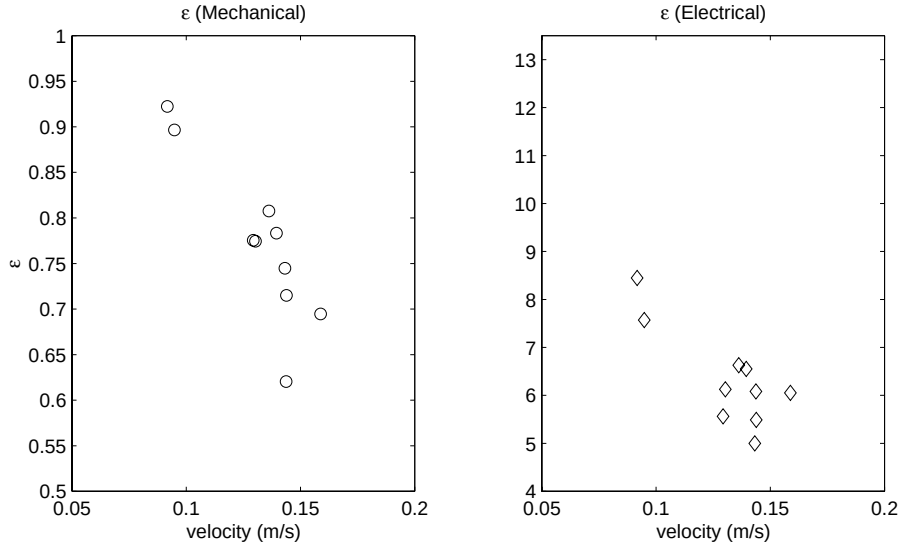

Figure 5.17: Mechanical and electrical specific resistance for a set of 10 experimental runs.

5.5 Summary

This chapter presented findings from walking experiments on Scout. Although rocking was not realized, a new walking algorithm based on commanding constant hip velocity was proposed. This algorithm was stable within a small region of operating conditions. An analysis of gathered data helped to pin point previously unmodeled dynamical effect helping to explain discrepancies between experiment and simulation. In addition, electrical and mechanical specific resistances were measured. Specific resistance measurements for Scout II, based on mechanical power, matched those of Monopod II, one of the most efficient robots to date. This suggests that if Scout's design can be refined, it may become a truly useful legged robotic platform for research and real world applications.

Chapter 6

Conclusion

This thesis presented research on the successful development of a dynamic compliant walking algorithm for the Scout II robot. This was achieved using a simple open loop control strategy that commanded constant hip velocity during periods of leg stance and two decoupled leg state machines to synchronise leg actions.

The success of this simple controller parallels previous findings at McGill's Ambulatory Robotics Lab (ARL), showing that seemingly complex behaviours can be achieved using simple control strategies. Understanding the limits of this approach is the first step in producing truly useful and versatile robots.

The help gain a better understanding of dominant dynamical factors influencing robot locomotion, an iterative approach of simulation, analysis, and experimentation was used. This approach has motivated the following conclusions:

- Mechanical complexity is not a requisite for obtaining complex locomotory behaviour from a walking robot. This said, it is unlikely that a single robot will accommodate all gaits with the same energetic efficiency. In particular, a design such as Scout's that does not use knees, is better suited for running rather than walking gaits. This is supported

by the fact that running gaits can use ballistic phases of motion to store greater amounts of energy in leg springs. Vertical energy can thus be re-introduced into locomotion, without the need for the large touchdown angles used in walking. Furthermore, given the touchdown impacts seen in running, larger toe/ground normal forces also develop, helping to reduce the occurrence of slip during stance.

- Scout's walking gait could be much improved with the redesign of the robot's legs. In particular reducing sliding friction would help make both walking and running more efficient. This would also allow locomotion controllers to take full advantage of the system's unforced response, helping to simplify control algorithms. Strategies such as the natural frequency rocking and walking controllers developed in chapter 4 could then be used. In the area of running, reducing sliding friction would most likely increase maximum achievable speeds and pitching amplitude, two desirable qualities for rough terrain locomotion. Until the robot's leg design is modified, future simulations should incorporate sliding friction effects in prismatic leg models. Leg deflection tests such as those described in section 5.2 could be used to yield estimates of Coulomb leg friction.

- Having found the significant effect variations in supply voltage can have on motor torque/speed limitations and on the controller effectiveness, future work should use more conservative estimates of achievable torque, both in simulation and experiment. Doing this should not only help to bring simulation and experimental results in tighter correspondence with one another. Robot design alternatives also exist to help improve these characteristics. A reevaluation of the power supply system on Scout may warrant increasing the robot's operation voltage to expand the polygon of torques that may be applied for a given leg speed. A safer approach might be to find a way of reducing voltage variations in the system. Having said this, these hardware modifications would not magically solve the torque/speed constraints Scout currently faces, since increasing torque during leg slip, would aggravate the problem

rather than help to solve it.

As is the case with most research, results always produce more new questions than answers. Interesting avenues for future research include:

- Attempts to further simplify the developed walking controller. If a version of the proposed constant hip velocity controller can be implemented using only proprioceptive sensing, that is, controlling the relative angle between legs and body, instead of the leg angle with respect to vertical, this may allow for the design of an even simpler legged robot platform, through the elimination of redundant sensing.

- A comparative study of walking versus running energetics on Scout II. This would be an interesting way of learning more about system behaviour and formally identifying efficient locomotion modes for the robot.

- A study of gait transitions between walking and running. As mentioned power sensing hardware may allow transitions to occur autonomously once running energetics is better understood.

- Use of linear or rotary knee actuation. Given that walking and running are known to be achievable with Scout's current mechanical configuration, using only one actuated degree of freedom per leg, these extra actuators could help to provide additional control "knobs", helping to further refine current locomotion gaits.

Bibliography

[1] M. Ahmadi and M. Buehler. A control strategy for stable passive running. *Proc. IEEE/RSJ Int. Conf. Intelligent Systems and Robots*, pages 152–157, August 1995.

[2] M. Ahmadi and M. Buehler. The arl monopod ii running robot: Control and energetics. *Proc. IEEE Int. Conf. Robotics and Automation*, pages 1689–1694, May 1999.

[3] R. McN. Alexander. *Elastic Mechanims in Animal Movement*. Cambridge University Press, Cambridge, 1988.

[4] J. Bares, M. Hebert, T. Kanade, E. Krotkov, T. Mitchelland R. Simmons, and W. Whittaker. Ambler: An autonomous rover for planetary exploration. *IEEE Computer*, 22(6):18–26, June 1989.

[5] J. Bares and David S. Wettergreen. Dante ii : Technical description, results, and lessons learned. *Int. J. Robotics Research*, 18(7):621–649, July 1999.

[6] R. Battaglia. Design of the scout ii quadruped with preliminary stair-climbing. Master thesis, McGill University, Montréal, Quebec, Canada, March 1999.

[7] F. P. Beer and E. R. Johnston Jr. *Vector Mechanics for Engineers DYNAMICS*. McGraw Hill Book Co., Toronto, 1988.

[8] M. D. Berkemeier. Approximate return maps for quadrupedal running. In *Proc. IEEE Int. Conf. Robotics and Automation*, volume 1, pages 805–810, Albuquerque, NM, April 1997.

[9] R. A. Brooks. A robust layered control system for a mobile robot. Technical report, MIT AI Memo 864, September 1985.

[10] M. Buehler, R. Battaglia, A. Cocosco, G. Hawker, J. Sarkis, and K. Yamazaki. Scout: A simple quadruped that walks, climbs, and runs. *Proc. IEEE Int. Conf. Robotics and Automation*, pages 1701–1712, 1998.

[11] M. Buehler, A. Cocosco, K. Yamazaki, and R. Battaglia. Stable open loop walking in quadruped robots with stiff legs. *Proc. IEEE Int. Conf. Robotics and Automation*, pages 2348–2353, May 1999.

[12] C. M. Chew, J. E. Pratt, and G. A. Pratt. Blind walking of a planar bipedal robot on sloped terrain. In *Proc. IEEE Int. Conf. Robotics and Automation*, Detroit, MI, 1999.

[13] A. Cocosco. Control of walking in a quadruped robot with stiff legs. Master thesis, McGill University, Montréal, Quebec, Canada, July 1998.

[14] J. J. Collins and I.N. Stewart. Coupled nonlinear oscillators and the symmetries of animal gaits. *Journal of Nonlinear Science*, 73:349–392, 1993.

[15] PC104 Consortium. *PC/104 Embedded-PC Modules.* http://www.pc104.org.

[16] Advanced Motion Controls. *PWM Servo Amplifiers Catalogue.* http://www.a-m-c.com/, 1992.

[17] SONY Corporation. *SONY World Homepage.* http://www.world.sony.com/, 2000.

[18] A. Daberkow, J. Gao, and W. Schielden. Walking without impacts. *CISM-IFToMM Symposium on the Theory and Practice of Robots and Manipulators*, pages 340–348, 1990.

[19] E. R. Dunn and R. D. Howe. Towards mooth bipedal walking. In *Proc. IEEE Int. Conf. Robotics and Automation*, pages 2489–2494, 1994.

[20] E. R. Dunn and R. D. Howe. Foot placement and velocity control in smooth bipedal walking. In *Proc. IEEE Int. Conf. Robotics and Automation*, pages 578–583, Minneapolis, MN, Apr 1996.

[21] M. H. Raibert et al. Dynamically stable legged locomotion. Technical Report CMU-LL-4-1985, Carnegie-Mellon University, 1985.

[22] G. Gabrielli and T. H. von Karman. What price speed ? *Mechanical Engineering*, 72(10):775–781, 1950.

[23] P. Gambayran. *How Mammals Run : Anatomical Adaptations*. John Wiley and Sons, Inc., New York, 1974.

[24] M. Garcia, A. Chatterjee, and A. Ruina. Speed, efficiency, and stability of small-slope 2-d passive dynamic biped walking. In *Proc. IEEE Int. Conf. Robotics and Automation*, Leuven, Belgium, May 1998.

[25] A. Goswami. Foot rotation indicator (fri) point: A new gait planning tool to evaluate postural stability of biped robots. In *Proc. IEEE Int. Conf. Robotics and Automation*, pages 47–52, Detroit, MI, May 1999.

[26] A. Goswami. Postural stability of biped robots and the foot rotation indicator (fri) point. *Int. J. Robotics Research*, 18(6), 1999.

[27] P. Gregorio. Design, control and energy minimization strategies for an electrically actuated legged robot. Master's thesis, McGill University, Montréal, Quebec, Canada, August 1994.

[28] P. Gregorio, M. Ahmadi, and M. Buehler. Design, control, and energetics of an electrically actuated legged robot. *IEEE Trans. Systems, Man, and Cybernetics*, 27B(4):626–634, August 1997.

[29] S. Grillner. Neurobiological bases of rhythmic motor acts in vertebrates. *Science*, 228:143–149, 1985.

[30] K. Sakurama H. Kimura and S. Akiyama. Dynamic walking and running of the quadruped using neural oscillator. In *Proc. IEEE/RSJ Int. Conf. Intelligent Systems and Robots*, pages 50–57, Victoria, October 1998.

[31] G. Hawker and M. Buehler. Quadruped trotting with passive knees - design, control, and experiments. *Proc. IEEE Int. Conf. Robotics and Automation*, April 2000.

[32] K. Hirai, M. Hirose, Y. Haikawa, and T. Takenaka. The development of Honda humanoid robot. In *Proc. IEEE Int. Conf. Robotics and Automation*, pages 1321–1326, Leuven, Belgium, 1998.

[33] D. F. Hoyt and C. R. Taylor. Gait and the energetics of locomotion in horses. *Nature*, 292:239–240, 1981.

[34] Associated Spring Raymond. Barnes Group Inc. *SPEC : Stock Springs, Spring Washers and Retaining Rings*. http://www.barnesgroupinc.com/, 1995.

[35] G. A. Pratt J. E. Pratt, P. Dilworth. Virtual model control of a bipedal walking robot. In *Proc. IEEE Int. Conf. Robotics and Automation*, pages 193–198, Albuquerque, NM, April 1997.

[36] H. Kimura. Realization of dynamic walking and running of the quadruped using neural oscillator. In *5th Int. Conf. on Simulation of Adaptive Behavior (SAB98), Workshop on Biological Inspired Walking*, pages 7–15, Zurich, 1998.

[37] H. Kitano, M. Fujita, S. Zrehen, and K. Kageyama. Sony legged robot for robocup challenge. volume 3, pages 2605–2612, 1998.

[38] QNX Software Systems Ltd. *QNX TCP/IP Users Guide*. 1994.

[39] K. Matsuoka. Sustained oscillations generated by mutually inhibiting neurons with adaptation. *Biological Cybernetics*, 52:367–376, 1985.

[40] T. McGeer. Passive dynamic walking. *Int. J. Robotics Research*, 9(2):62–82, 1990.

[41] T. McGeer. Passive walking with knees. In *Proc. IEEE Int. Conf. Robotics and Automation*, pages 1640–1645, Cincinnati, OH, May 1990.

[42] R. McGhee and K. Waldron. The adaptive suspension vehicle project: A case study in the development of an advanced concept for land locomotion. In *Unmanned Systems*, pages 34–43, Summer 1985.

[43] R. B. McGhee and A. A. Frank. On the stability properties of quadruped creeping gaits. *Mathematical Biosciences*, 3:331–351, 1968.

[44] D. A. Messuri and C. A. Klein. Automatic body regulation for maintaining stability of a legged vehicle during rough terrrain locomotion. In *Proc. IEEE Int. Conf. Robotics and Automation*, pages 132–141, 1985.

[45] E. Muybridge. *Animals in Motion.* Dover Publications, Inc., New York, 1957.

[46] P. V. Nagy, S. Desa, and W. L. Whittaker. Energy-based stability measures for reliable locomotion of statically stable walkers : Theory and application. *Int. J. Robotics Research*, RA-1(3):272–287, 1994.

[47] A. Neishtadt and Z. Li. Stability proof of raibert's four-legged hopper in bounding gait. Technical Report 578, New York University, Courant Institute, New York, N.Y., Sep 1991.

[48] D. Papadopoulos. Stable running for a quadruped robot with compliant legs. Master's thesis, McGill University, Montréal, Quebec, Canada, February 2000.

[49] D. Papadopoulos and M. Buehler. Stable running in a quadruped robot with compliant legs. *Proc. IEEE Int. Conf. Robotics and Automation*, April 2000.

[50] J. E. Pratt. Virtual model control of a biped walking robot. Master thesis, Massachusetts Institute of Technology, August 1995.

[51] J. E. Pratt and G. A. Pratt. Exploiting natural dynamics in the control of a planr biped walking robot. In *Proceedings of the Thity-Sixth*

Annual Allerton Conference on Communicatio, Control and Computing, Monticello, IL, 1998.

[52] J. E. Pratt and G. A. Pratt. Intuitive control of a planar bipedal walking robot. In *Proc. IEEE Int. Conf. Robotics and Automation*, Leuven, Belgium, 1998.

[53] J. E. Pratt, A. Torres, P. Dilworth, and G. A. Pratt. Virtual actuator control. In *Proc. IEEE/RSJ Int. Conf. Intelligent Systems and Robots*, Osaka, Japan, 1996.

[54] M. H. Raibert. *Legged Robots That Balance.* MIT Press, 1986.

[55] M. H. Raibert. Trotting, pacing, and bounding by a quadruped robot. *J. of Biomechanics*, 1991.

[56] Knowledge Revolution. *Working Model 2D User's Guide.* San Mateo, California, 1996.

[57] R. Ringrose. Self-stabilizing running. In *Proc. IEEE Int. Conf. Robotics and Automation*, Albuquerque, NM, May 1997.

[58] M. L. Shik, F. V. Severin, and G. N. Orlovsky. Control of walking and running by means of electrical stimulation to the mid-brain. *Biophysics*, 11:756–765, 1966.

[59] I. E. Sutherland and M. K. Ullner. Footprints in the asphalt. *Int. J. Robotics Research*, 3(2):29–36, 1984.

[60] G. Taga. A model of the neuro-musculo-skeletal system for human locomotion ii - real-time adaptability under various constraints. *Biological Cybernetics*, 73:113–121, 1995.

[61] G. Taga, Y. Yamaguchi, and H. Shimizu. Self-organized control of bipedal locomotion by neural oscillators in unpredictable environment. *Biological Cybernetics*, 65:147–159, 1991.

[62] W. Thompson. *Theory of Vibration with Applications, Fourth Edition.* Prentice Hall, Englewood Cliffs, New Jersey, 1993.

[63] M. Vukobratović and D. Juricic. Contributions to the synthesis of biped gait. *IEEE Trans. Biom. Eng.*, BME-16:1–6, 1969.

[64] K.S. Yamazaki. The design and control of scout i, a simple quadruped robot. Master thesis, McGill University, Montréal, Quebec, Canada, February 1999.

Appendix A

MPC550 Interface Schematics

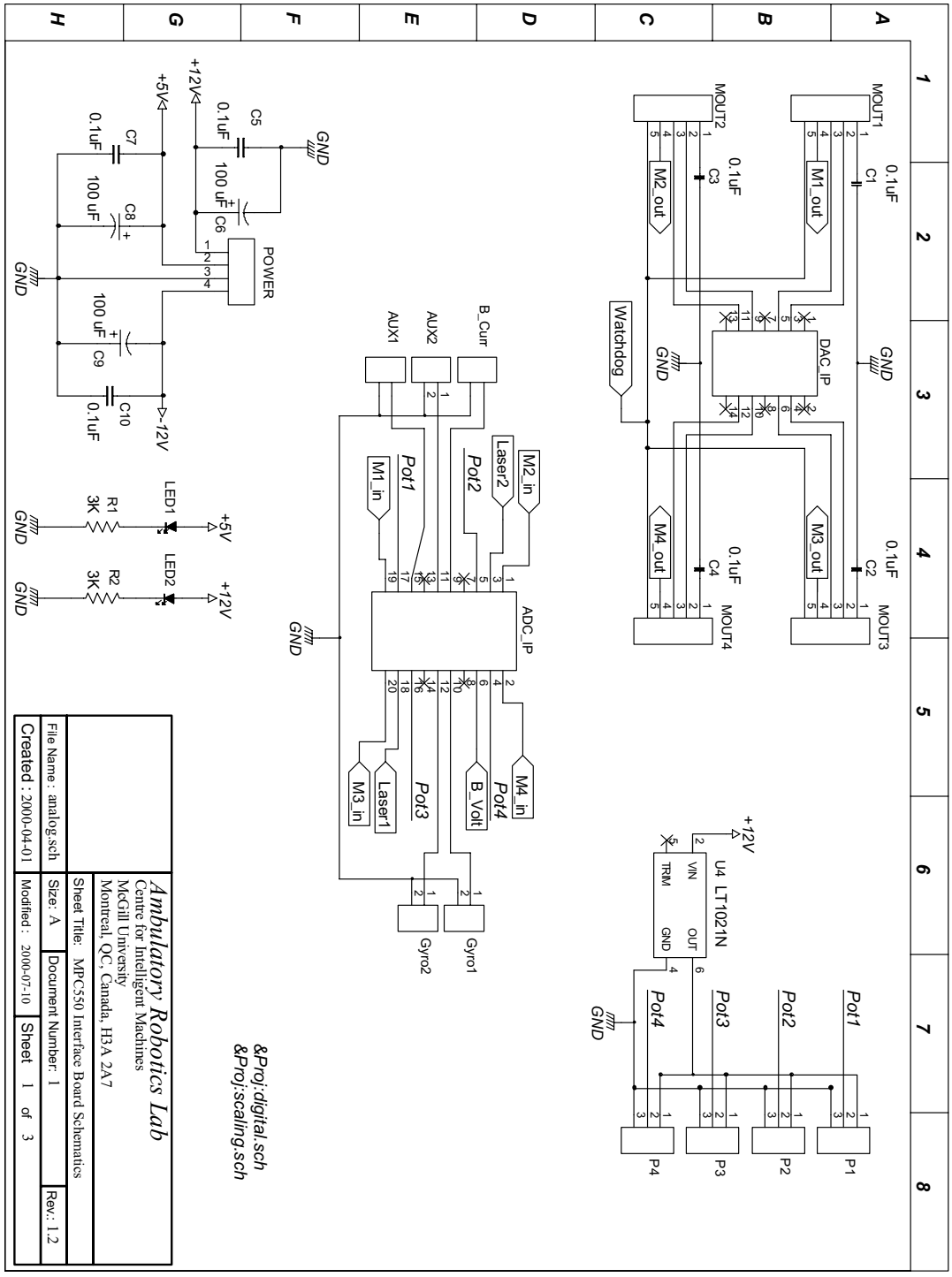

Figure A.1: MPC550 Interface Schematics - 1/3

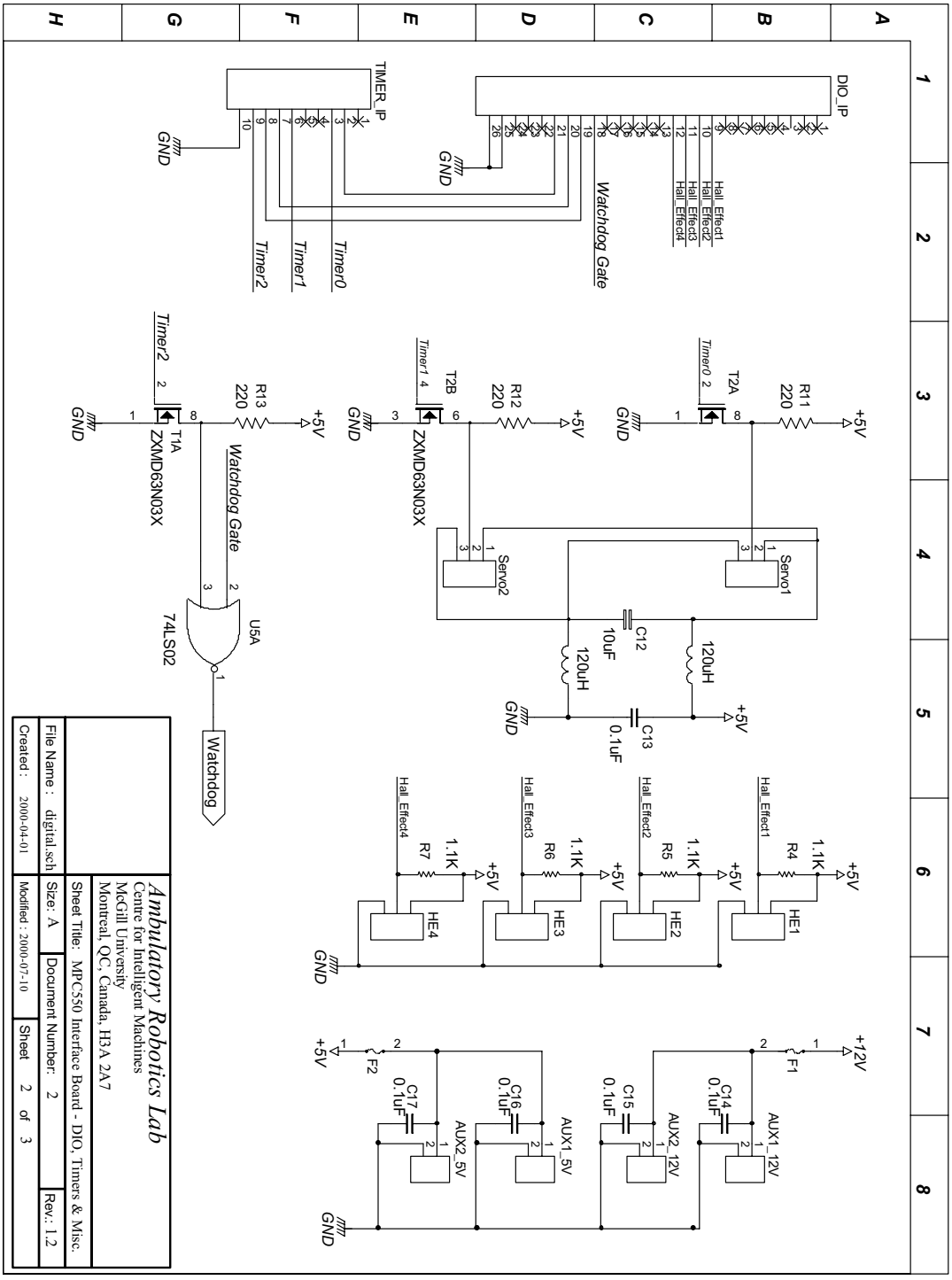

Figure A.2: MPC550 Interface Schematics - 2/3

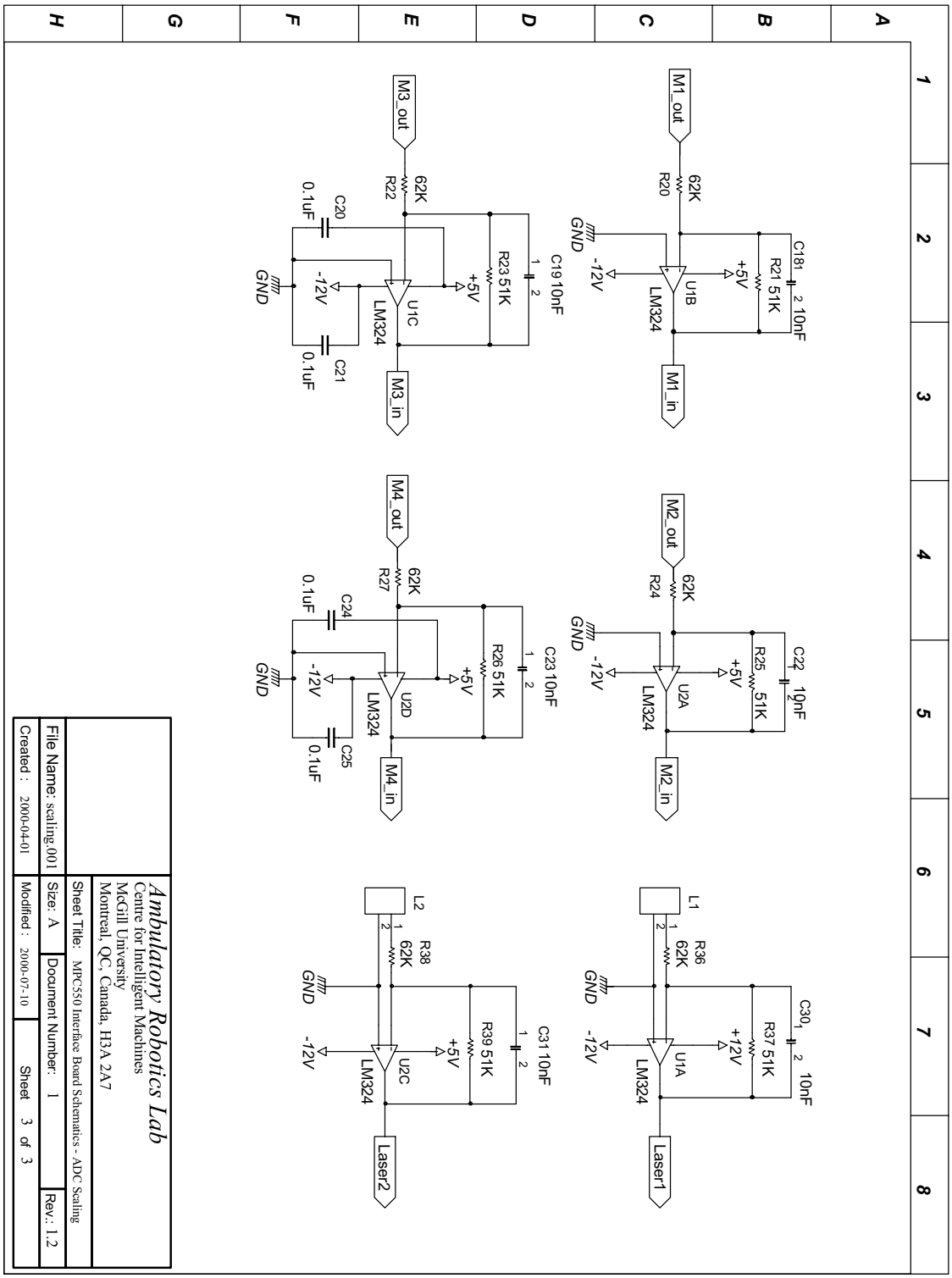

Figure A.3: MPC550 Interface Schematics - 3/3